Available online at www.sciencedirect.com
ScienceDirect
Sedimentary Geology 192 (2006) 75–98
Sedimentary Geology
www.elsevier.com/locate/sedgeo

Sedimentology and geochemistry of extensive very coarse deepwater submarine fan sediments in the Middle Jurassic of Oman, emplaced by giant tsunami triggered by submarine mass flows

M.E. Brookfield [a,*], I. Blechschmidt [b,1], R. Hannigan [c,2], M. Coniglio [d,3], B. Simonson [e,4], G. Wilson [a]

[a] *Land Resource Science, Guelph University, Guelph, Ontario, Canada N1G 2W1*
[b] *University of Bern, Institute of Geological Sciences, Baltzerstrasse 1-3, CH-3012 Bern, Switzerland*
[c] *Department of Chemistry and Physics, Arkansas State University, AR 72467, USA*
[d] *Department of Department of Earth Sciences, University of Waterloo, Waterloo, Ontario, Canada N2L 3G1*
[e] *Geology Department, Oberlin College, Oberlin, OH 44074, USA*

Received 13 October 2004; received in revised form 10 March 2006; accepted 30 March 2006

Abstract

Unusual fining upwards coarse conglomerates overlain by sandstones, thin cherts and green shales occur at the top of the deep-water submarine fan deposits of the Oolitic Limestone Member of the Jurassic Guwayza Formation of Oman. They separate the dominantly submarine fan deposits of the Guwayza Formation from the pelagic shales, fine-grained limestones and cherts of the overlying Sidr Formation. The cross-bedded and graded framework conglomerates occur in extensive, tabular units and are dominated by earlier Mesozoic carbonate clasts with sandy oolitic and peloidal grains derived from fault escarpments and shelf sediments far to the southwest. Subordinate inverse grading, very thick beds, very large floating clasts (up to 100 m long in places) indicate deposition from catastrophic debris flows. Though most palaeocurrents indicate flow from off the platform to the southwest, hummocky cross-bedding shows divergent palaeocurrents suggesting movement in part by deep-water waves. The beds are too coarse for antidune formation and the conglomerate to sand hummocks indicate decelerating flow. There are no nearby large objects to deflect turbidity currents to form divergent flows. We consider that the hummocky cross-stratification, like that in shallow water, was formed by interfering waves. That such coarse, tabular conglomerates affected by wave action occur over extensive areas across deep submarine fan environments, suggests deposition by high-velocity seaward-moving debris and grain flows followed by reworking by waves large enough to redistribute coarse sediment in deep water. The only waves large enough are those of giant tsunami. Petrology and geochemistry show no impact or explosive volcanic constituents in the finer units and the waves involved are too large for

* Corresponding author. Tel.: +1 519 824 4120x2654.
E-mail addresses: mbrookfi@lrs.uoguelph.ca (M.E. Brookfield), blechschmidt@geo.unibe.ch (I. Blechschmidt), hannigan@mail.astate.edu (R. Hannigan), coniglio@sciborg.uwaterloo.ca (M. Coniglio), bruce.simonson@oberlin.edu (B. Simonson).
[1] Tel.: +41 31 631 87 73.
[2] Tel.: +1 870 972 3089.
[3] Tel.: +1 519 888 4567x2066.
[4] Tel.: +1 440 775 8347.

0037-0738/$ - see front matter
doi:10.1016/j.sedgeo.2006.03.026

generation directly by submarine fault displacements. We suggest that the top Guwayza conglomerates were deposited by very large submarine slides which were then reworked by the tsunami generated by them. Such contemporary massive slope failure deposits are present on the adjacent slope and shelf margin.

Keywords: Tsunami; Deposits; Jurassic; Oman

1. Introduction

During the Late Cretaceous in northeastern Oman, the former Mesozoic passive margin and adjacent sea-floor was thrust southwestwards in a series of great nappes to form the Oman mountains (Glennie et al., 1974; Cooper, 1988), in one of the major episodes of giant ophiolite nappes emplacement in the geological record (Brookfield, 1977) (Fig. 1A). In these nappes, successively more distal units were stacked generally in order, so that the vertical succession of nappes represents (with some variation

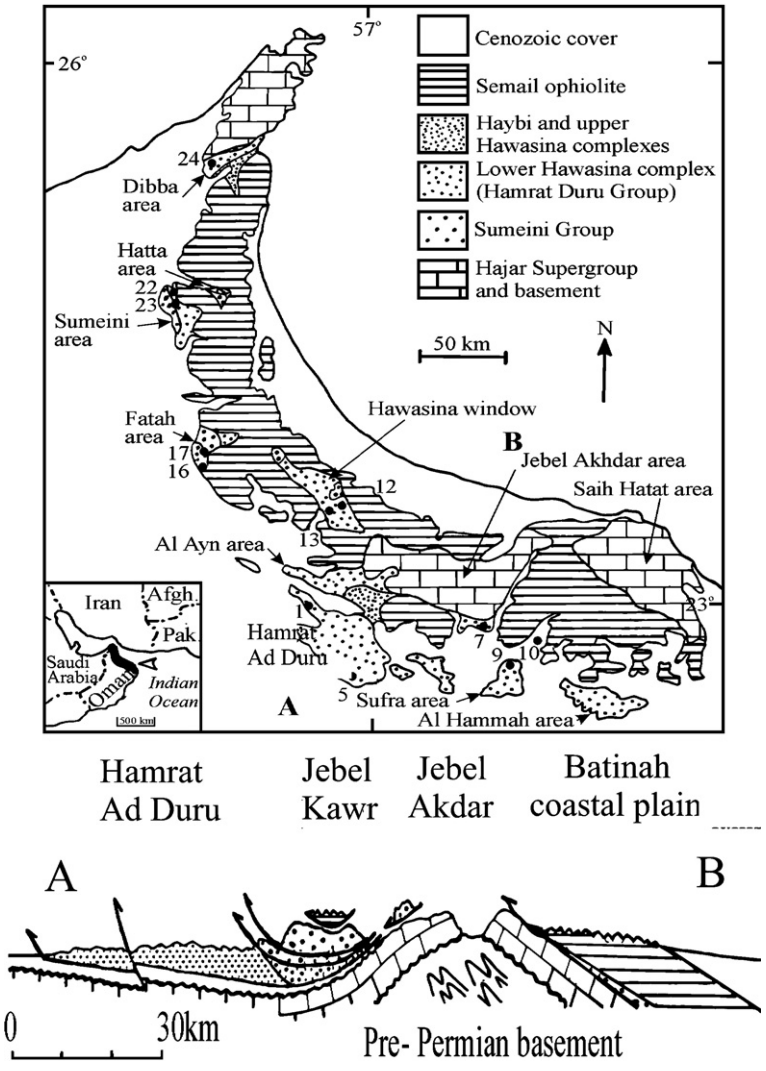

Fig. 1. (A) Geological map of northern Oman; structural units, location of sections (Cooper, 1990 numbers used) and A–B cross-section location: inset shows location of northern Oman on a map. (B) Structural cross-section across Hamrat Ad Duru and Jebel Akdar dome along line A–B.

due to out-of-sequence thrusting—see Searle, 1985) contemporaneous Mesozoic shelf, slope to oceanic environments (Fig. 1B). The Hawasina nappe complex is dominated by the late Permian–late Cretaceous Hamrat Duru Group which consists of diverse, predominantly deep-water marine shales, limestones, limestone conglomerates, sandstones and radiolarian cherts about 1 km thick deposited northeast of, and adjacent to, the Oman passive margin during the Mesozoic (Glennie et al., 1974; Béchennec et al., 1988; Blechschmidt, 2002; Blechschmidt et al., 2004) (Fig. 2). The Group was deposited off the passive margin as predominantly slope and basin submarine fan deposits between the Arabian shelf and upper slope (Sumeini Group) environments and a group of oceanic seamounts which now lie as exotic blocks beneath the ophiolite (Watts and Garrison, 1986; Robertson and Searle, 1990; Pillevuit et al., 1997). Palinspastic restoration of the thrust sheets shows the Hamrat Ad Duru slope and basin fan deposits flanked by the shelf-edge Sumeini Group and the deeper marine Haybi Group (Fig. 3A, B).

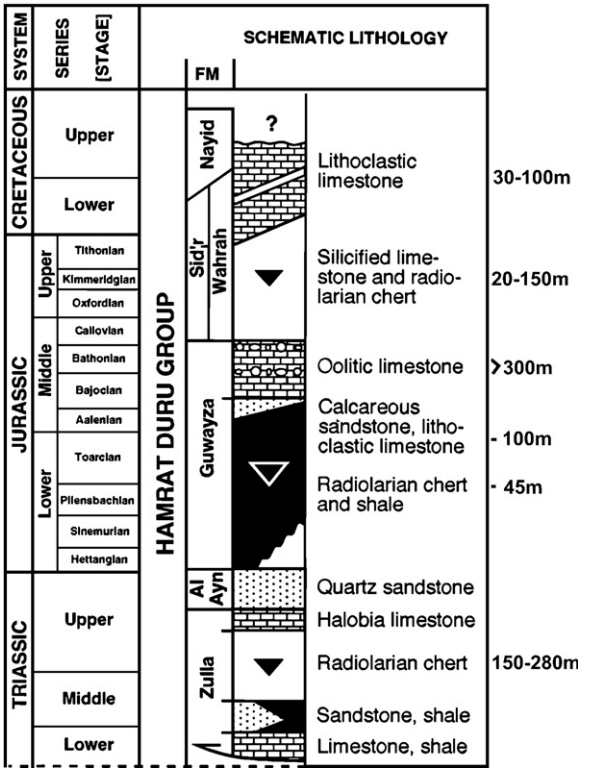

Fig. 2. Stratigraphy of the Hamrat Duru Group (from Blechschmidt, 2002; Blechschmidt et al., 2004).

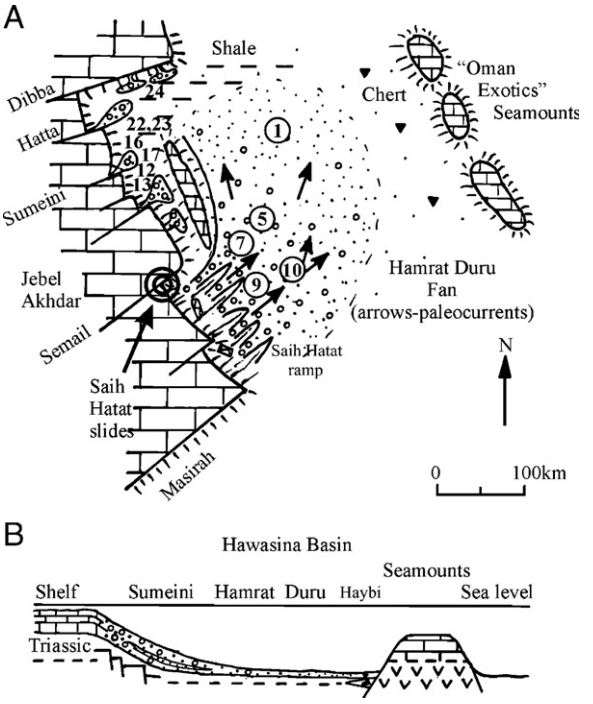

Fig. 3. (A) Palaeogeographic map of the Oman passive margin during deposition of the Guwayza Formation in the Middle Jurassic, with inferred depositional locations of structural units and sections (Figs. 1 and 4): (Hamrat Ad Duru sections are circled and location of Saih Hatat slides is double-circled (based on Cooper, 1990; Robertson and Searle, 1990). (B) Restored cross-section of Jurassic Oman passive margin with inferred original positions of structural units (based on Robertson and Searle, 1990).

The purpose of this paper is to describe and interpret an areally persistent coarse conglomeratic unit which caps the mid-Jurassic Guwayza Formation.

2. Guwayza formation: stratigraphy and palaeoenvironment

The stratigraphic terminology follows Blechschmidt et al. (2004). The Guwayza Formation (?Pliensbachian to Callovian in age) consists of more than 500 m of radiolarian chert and shale, calcareous sandstone and lithoclastic limestone, and oolitic limestone (Fig. 2). The lower Tawi Sadh Member, up to 150 m thick, is highly variable and in places dies out altogether. The lower part consists of shale, radiolarian chert and silicified limestone which passes up into an upper part consisting of calcareous turbidite sandstones. Radiolaria indicate a late Pliensbachian(?) to early Toarcian age for the lower part and early to middle Bajocian for the upper part (Blechschmidt, 2002; Blechschmidt et al., 2004). The upper Oolitic Limestone Member consists of more than 300 m of oolitic, peloidal and lithoclastic carbonates in

three graded coarse- to fine-grained carbonate units interbedded with two finer-grained carbonate units (Blechschmidt et al., 2004) and was studied in some detail by Cooper (1989, 1990). The fauna indicate a late Bajocian to early Callovian age (Blechschmidt et al., 2004). The upper Tawi Sadh and Oolitic limestone members therefore represent coarser sediment inputs into deeper water, dominantly pelagic, sediments during the Middle Jurassic.

In the Hamrat Ad Duru allochthon, the Oolitic Limestone Member shows considerable lateral variation, but with a clear pattern of thinning (both in total and bed thickness) and fining (from conglomerate to sandy limestone) from south to north (Fig. 4). South of Jebel Akhdar (loc. 7, Fig. 4) in the most complete proximal section, it is more than 300 m thick and consists of amalgamated metre-thick beds of coarse graded calcarenite dominated by resedimented oolitic and lithoclastic material, and separated by fine-grained detrital carbonate. Carbonate conglomerates in the middle and upper parts of the Member consist of channelized fining-upwards grain-supported thick-bedded carbonate breccia and conglomerate, with sub-rounded to rounded clasts and large blocks of reef and lagoonal limestones in oolitic sand matrices (Cooper, 1989).

Sections in the central Hawasina window and Fatah areas (locs. 12 to 17, Fig. 4) have more shale and fewer conglomerates, contain matrix-supported debris flows with highly variable current indicators and show considerable lateral variation on a 100 metre to kilometre scale: Cooper (1990) interpreted these as deposits of a sub-basin separated by a subsided shelf block from the main southern fan. Although there is no capping conglomerate in the Hawasina window and Fatah areas, there is a sharp, possibly disconformable, change to radiolarian cherts of the overlying Sidr Formation (Watts, 1990).

In the more northerly Sumeini, Hatta and Dibba areas (locs. 22 to 24, Fig. 4), the Oolitic Limestone Member is capped by a coarse clast-supported conglomerate horizon, as in the south, except where there is a sudden, possibly disconformable, change to the radiolarian cherts of the Sidr Formation (Robertson et al., 1990a,b). In the Dibba area, the conglomerates contain boulders up to 5 m in diameter of algal limestone, reef limestone, fine-

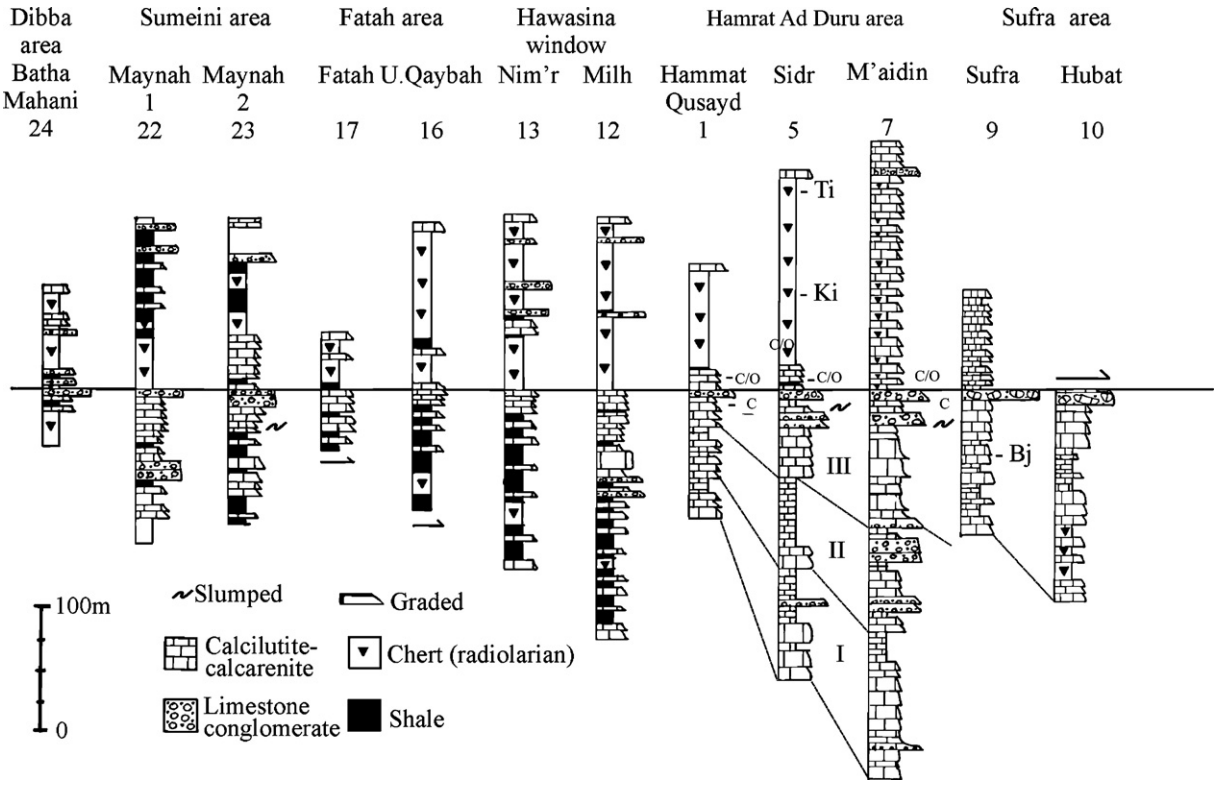

Fig. 4. Typical sections through the Guwayza and Sidr Formations (modified from Cooper, 1989, with his section numbers used): locations in Fig. 1. Subdivisions with Roman numbers on sections 1 to 10 are Cooper's (1990) cycles: letters at side are radiolarian-determined ages; Bj—Bajocian, Ba—Bathonian, C—Callovian, O—Oxfordian, Ki—Kimmeridgian, Ti—Tithonian.

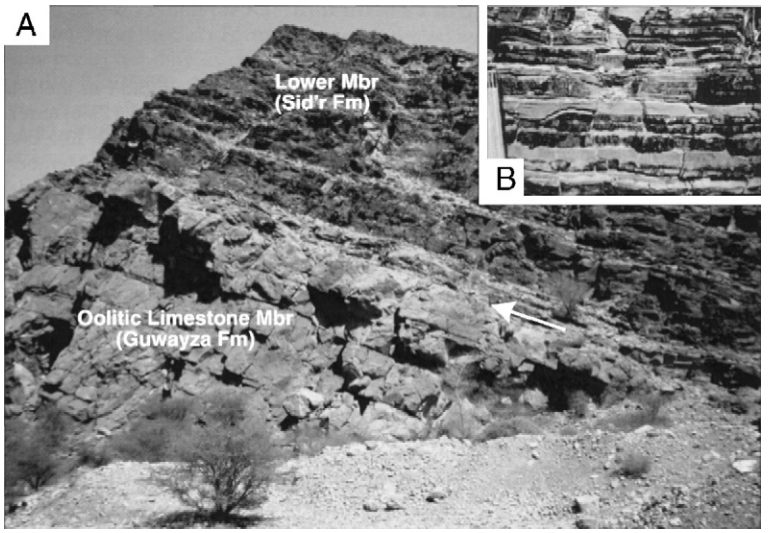

Fig. 5. Sharp contact between the Oolitic Limestone Member of the Guwayza Formation and overlying Sidr Formation, Al Sawad (loc. 7).

grained limestone, shale, green siltstone, and rare quartzite, sandstone and well-rounded granite boulders (Robertson et al., 1990a). Though these may have been derived from exposed basement along one of the faults, the rounded granites suggest subaerial weathering and thus a coastal source. Furthermore, these basement clasts are NOT found in more proximal slope units of the Sumeini Group (Fig. 3), suggesting that they were derived from shallow water via canyons (Robertson et al., 1990b). North of the Dibba area, the Middle Jurassic shelf deposits consist of 370 m of micritic algal limestones passing up into coral packstones, disconformably overlain by deep-water Berriasian siliceous limestones

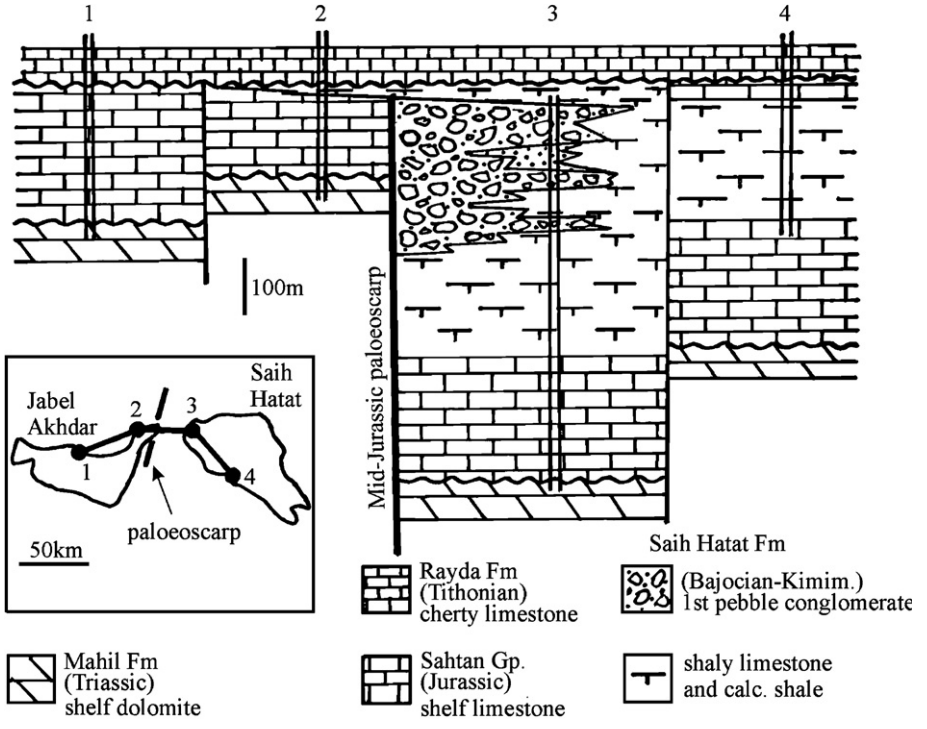

Fig. 6. Reconstructed cross section across the Sumeini gap paleoscarp on the Jurassic Oman shelf margin (based on Pratt and Smewing, 1990; their Figs 9 and 10). Numbered sections are basis for reconstruction. Location of slide double-circled in Fig. 4.

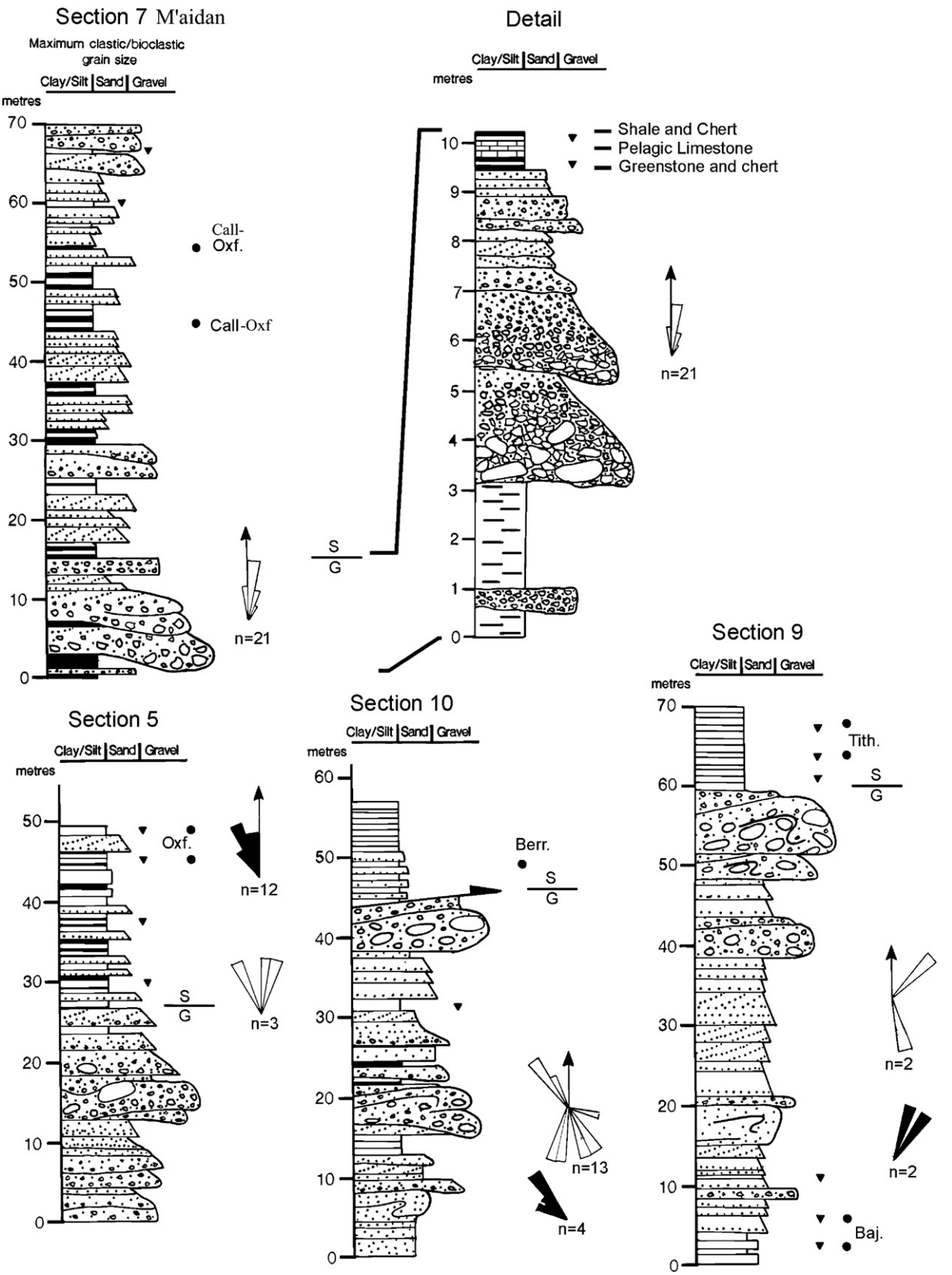
Section 7 M'aidan
Maximum clastic/bioclastic grain size
Clay/Silt | Sand | Gravel
metres
70
60
50
40
30
20
10
0
Call-Oxf.
Call-Oxf
n=21
Detail
Clay/Silt | Sand | Gravel
metres
10
9
8
7
6
5
4
3
2
1
0
Shale and Chert
Pelagic Limestone
Greenstone and chert
n=21
S
G
Section 5
Clay/Silt | Sand | Gravel
metres
50
40
30
20
10
0
Oxf.
n=12
n=3
S
G
Section 10
Clay/Silt | Sand | Gravel
metres
60
50
40
30
20
10
0
Berr.
S
G
n=13
n=4
Section 9
Clay/Silt | Sand | Gravel
metres
70
60
50
40
30
20
10
0
Tith.
S
G
n=2
n=2
Baj.

(Ricateau and Riche, 1980). Correlative coarse conglomeratic units occur in other structural units all along the Oman passive margin at the same stratigraphic level at the top of the Oolitic Limestone Member and its inferred equivalents, though dating is often too poor to prove synchroneity (Watts, 1990). Everywhere, there is a sharp (though sometimes transitional) contact with the overlying pelagic sediments of the Sidr Formation (Figs. 4 and 5).

On the Arabian shelf, sediments stratigraphically equivalent to the Oolitic Limestone Member lie within the Sahtan Group (Lower Jurassic to Tithonian) which also occurs as large inliers at Jebel Akhdar and Saih Hatat (Fig. 1). On Saih Hatat, deep-water clayey limestones enclose 400 m thick debris flow conglomerates with slump structures and overlie shallow water limestones, which indicates subsidence of at least part of the mid-Jurassic shelf at this time (Pratt and Smewing, 1990) (Fig. 6). The conglomerates are poorly sorted and contain subangular clasts up to 0.2 m in diameter of mixed shelf, slope and basin lithologies (radiolarian mudstones, oolitic grainstones, and Triassic dolomites). They occur as three units comparable to the three units at the top of the Oolitic Limestone member, and were shed from the faulted eastern edge of Jebel Akhdar (the Semail gap) where a NNE trending paleoscarp of Triassic dolomites is overlapped by younger Late Jurassic sediments. This suggests cumulative synsedimentary faulting of over 500 m and large-scale subsidence of the Saih Hatat platform area during deposition of the conglomerates, but how rapid this was is unknown (Fig. 6). On Jebel Akhdar, the autochthonous Sahtan Group (Lower Jurassic to Tithonian) consists of two thick units of quartz sandstones and sandy limestones sandwiching a relatively thin unit of nodular calcareous mudstones, but the top was eroded and a condensed reworked phosphatized horizon deposited beneath early Cretaceous cherty micritic limestones (Haan et al., 1990, Pratt and Smewing, 1990). Thus, over much of Arabian shelf adjacent to the Oman margin, a sudden change takes place from shallow to deep-water carbonate deposition sometime during the early Upper Jurassic (Callovian/Oxfordian).

The structurally highest units (upper Hawasina and part of Haybi complexes) contain sediments deposited between the Hawasina basin submarine fans and the seamounts represented by the Oman exotics (Searle and Graham, 1982; Robertson and Searle, 1990). The Oman exotics stand out as isolated, often vertical mountains composed of shallow marine, often reefal, dominantly Permian–Triassic limestones up to 1 km thick (Searle and Graham, 1982). They lie in complex melanges (Haybi Complex) immediately below the Semail ophiolite sheet, consist of carbonate facies not found on the contemporary Oman shelf and slope, and are sometimes underlain by thick intraplate alkali basalts (Pillevuit et al., 1997). The Haybi Complex contains breccias and megabreccias with reworked blocks and megablocks of Permian and Triassic shallow water carbonates derived from the seamounts in both Lower Jurassic and Lower Cretaceous Formations (Béchennec et al., 1988). However, there appear to be no breccia horizons in the mid-Jurassic correlative with the Oolitic Limestone Member. In the Oman exotics, Jurassic (early Jurassic to Tithonian) condensed pelagic carbonates (less than 2 m thick) rest disconformably on hardgrounds on thick Triassic (Ladinian–Norian) shallow water carbonates. And within the thin Jurassic, Upper Oxfordian to Tithonian cherty limestones rest abruptly on early Jurassic to late Bajocian or younger platy ammonite-bearing (ammonitico rosso) limestones (Pillevuit et al., 1997). The seamounts were therefore already in deep water when the coarse conglomerates of the Oolitic Limestone Member were being deposited, and this time period corresponds to non-deposition and corrosion on the seamounts.

2.1. Interpretation

All the sedimentary features of the Oolitic Limestone Member suggest deposition by mass flows and turbidity currents in a channelized submarine fan system extending outwards from the adjacent Oman carbonate platform (Cooper, 1989, 1990; Blechschmidt et al., 2004) (Fig. 3). In this southern part of the Hawasina allochthon, the palaeocurrents in the Oolitic Limestone Member show a swing from north and northeast in the south to more variable northwest to east in the north, with sources predominantly from the faulted southeastern Saih Hatat block (Fig. 3A).

The evidence from the Oman shelf and slope environments suggest major disruptions to sedimentation at the end of the Middle Jurassic (mid- to late Callovian, around 160 ma), at a time when quiet deeper

Fig. 7. Sections through the top Guwayza and lower Sidr Formations in the Hamrat Ad Duru and Sufrat areas (locations in Fig. 1); with detailed section of top Guwayza conglomerates at M'aidan (Section 7). Inverted solid triangles are radiolarian chert beds: dots with Oxf., etc., are dated Jurassic radiolarian horizons (from Blechschmidt, 2002; Blechschmidt et al., 2004). Rose diagrams are Palaeocurrents based on cross-bedding (blank) and sole marks (filled). Locations of following photograph figures noted.

water sedimentation on the seamounts ceased. One such disruption event is marked by the fault-related conglomerates on Saih Hatat and the widespread top conglomerate horizon of the Oolitic Limestone Member of the Guwayza Formation.

3. Top conglomerates of oolitic limestone member

The top of the Oolitic Limestone Member is marked by a very extensive coarse conglomeratic unit which is sharply overlain by the deep-water pelagic limestones and cherts of the late Callovian/Oxfordian to Albian/? Cenomanian Sidr or Wahrah Formations, marking a sharp drop in lithoclastic input to the basin (Figs. 2 and 5).

3.1. Description

The top conglomerate horizon occurs as almost tabular layers over at least hundreds to thousands of square kilometres in the Hamrat Ad Duru region. It can be traced easily for more than 25 km along the base of Jebel Akhdar and reappears in the Sumeini and Dibba areas far to the north (Figs. 3 and 4). It appears to have the same stratigraphic and sedimentological relationships along the entire Oman mountain range where present (Cooper, 1990). The youngest fossils in beds below the top conglomerates indicate an early Callovian age, while overlying cherts of the Sidr Formation contain Callovian/Oxfordian radiolaria. A mid- to late Callovian age is therefore probable for the top conglomerates (Blechschmidt et al., 2004). However, we depend to a great extent on the sharp break between the Guwayza and Sidr formations for correlation. This seems reasonable from a sequence stratigraphic point of view. However, if this sharp break can be shown to be diachronous, at least in the Hamrat Ad Duru region, then many of our sedimentological conclusions are suspect.

We studied the top conglomerate in the Hamrat Ad Duru area. The well-developed thinning- and fining-upward section of the top conglomerate is a regional feature seen at all outcrops, though there is significant variation in detail (Fig. 7) and the top conglomerate horizon regionally truncates the channelized fan units in the underlying part of the Oolitic Limestone Member (Fig. 4).

In most areas, the conglomeratic horizon consists of several (three at M'aidan, Fig. 8A; the variations due to amalgamation in places) fining upwards units starting with a thick-bedded, poorly to moderately sorted, clast-supported conglomerate (1 to 5 m thick) (Fig. 9), with boulder to pebble-sized clasts in a medium to coarse grained oolitic grainstone matrix. Each conglomerate is

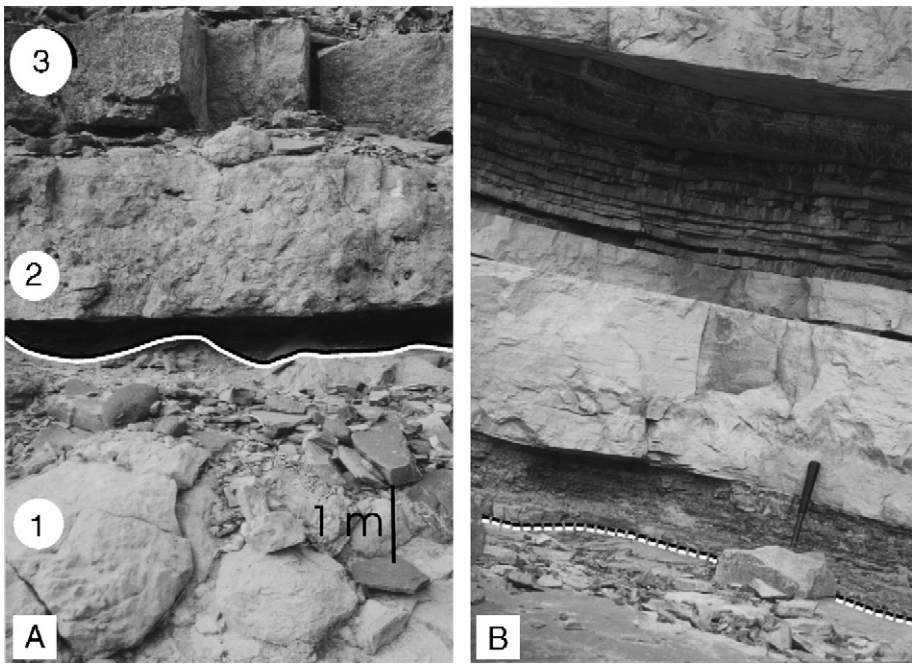

Fig. 8. Topmost conglomerates at M'aidan (loc. 7): (A) Three generally fining and thinning upwards conglomerates (numbered 1 to 3) each overlain by thin greenish shale, chert and pelagic limestone; (B) green shale and chert (30 cm) overlying third graded conglomerate and itself overlain by interbedded fine-grained detrital limestones and cherts of the Sidr Formation. Dashed line is top of uppermost conglomerate Hammer handle is 30 cm long.

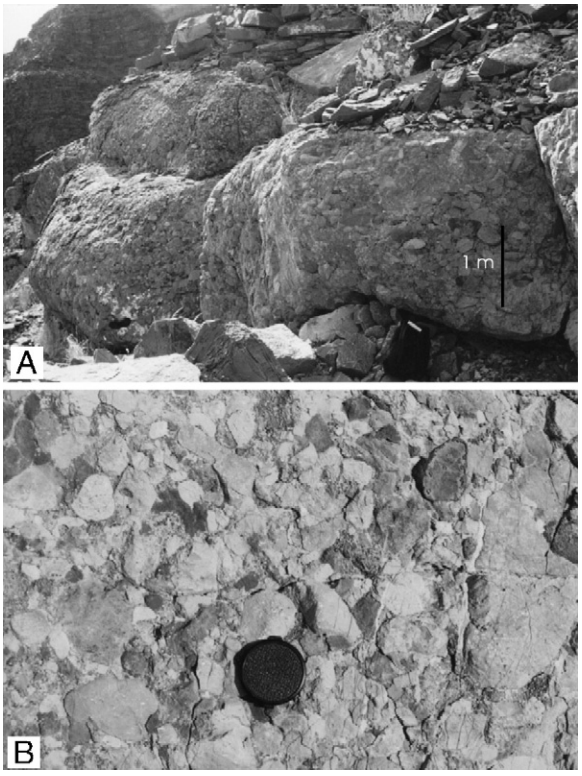

Fig. 9. Topmost conglomerate at M'aidan (loc. 7): (A) Section of conglomerate #1 (Fig. 8A) showing framework texture, grading, moderate sorting and predominance of rounded dolomite clasts (with location of B); (B) detail of A, vertical section of rounded–subrounded moderately sorted framework conglomerate (camera lens cap is 5 cm diameter).

a poorly organized, fining upward unit. The topmost shale above the third conglomerate is directly overlain by the pelagic cherty limestones and cherts of the Sidr Formation (Fig. 8B). Most of the sandy matrix (and the carbonate grainstones above) consists of contemporary shelf-derived moderately sorted ooid- and ooid-intraclastic grainstones to poorly sorted ooid-bioclastic–intraclastic grainstones and ooid-peloidal intraclastic grainstones (Fig. 10). Compound ooids and grapestone aggregates typical of very shallow water are present but are rare. The conglomerates frequently contain very large clasts floating in a disorganized fabric concentrated towards the top of the conglomeratic parts (Fig. 11). The clasts are predominantly subrounded to rounded Triassic and Jurassic dolomites and other carbonate clasts, particularly shallow-water oolites, but rare basalt clasts occur (Fig. 12A) and some clasts are distorted deeper-water slope carbonates (Fig. 12B) (Blechschmidt et al., 2004). The nearest source for the shallow-water lithologies was either several hundred kilometres to the southwest before late Cretaceous thrusting (Pratt and Smewing, 1990) or from older Triassic–mid Jurassic units exposed along the shelf-margin faults such as those on and marginal to Saih Hatat (Fig. 3).

At M'aidin (Fig. 7 Section 7), the lowermost slightly graded bed (up to 3 m thick) consists of poorly to well-rounded cobble-sized clasts with boulders up to 1.8 m diameter in an oolitic grainstone matrix. The overlying slightly graded cross-bedded conglomerate (1.5 m thick) consists of moderately sorted cobble-sized clasts passing up into cross-bedded pebbly grainstones with aligned pebbles and trough cross-lamination. The uppermost graded conglomerate and conglomeratic sandstone (25–50 cm thick) consist of poorly sorted granules and pebbles in a medium to coarse-grained oolitic matrix. Both the upper parts of the conglomerates and the sandstones show hummocky cross-stratification (Fig. 13). Many of the conglomerate and sand cross-beds also show divergent and sometimes completely reversed flow directions within the same bed (Figs. 7 and 13C).

Where the basal contacts are non-erosive, each conglomerate–grainstone unit is overlain by distinctive, thin greenish shale and chert layers (Fig. 8A). These green shales and cherts contain pelagic fossils but were also rapidly deposited (see geochemistry section) suggesting that they form part of the depositional events recorded by the conglomerates.

At Sufra and Hubat (locs. 9 and 10, Fig. 4), spectacularly well-exposed megabreccias with Permian to Triassic limestone blocks (up to 100 m long) also occur with slump-folded strata and metre-sized sand volcanoes (Cooper, 1990; Blechschmidt et al., 2004). Some of the clasts are pelagic ammonite-bearing limestones (Hallstat facies) which are highly condensed and form only on deep isolated carbonate blocks and not on normal Mesozoic shelves (Kuznetsov, 2003). The clasts thus come not only from the unstable Saih Hatat shelf and slope (Pratt and Smewing, 1990) but also from isolated blocks (one of which is shown in Fig. 3A) or possibly seamounts (Robertson, 1987).

3.2. Interpretation

Any interpretation of the topmost Oolitic Limestone Member conglomeratic horizon has to account for: its wide distribution, its tabular nature, its truncation of underlying channelized fan lobes, the hummocky cross-stratification, the pelagic shale and chert at the top of each bed, the evidence of rapid deposition of thick individual graded beds as mass flows, the volumes involved, the divergent palaeocurrents, and the dominance of far-traveled rounded carbonate pebbles and

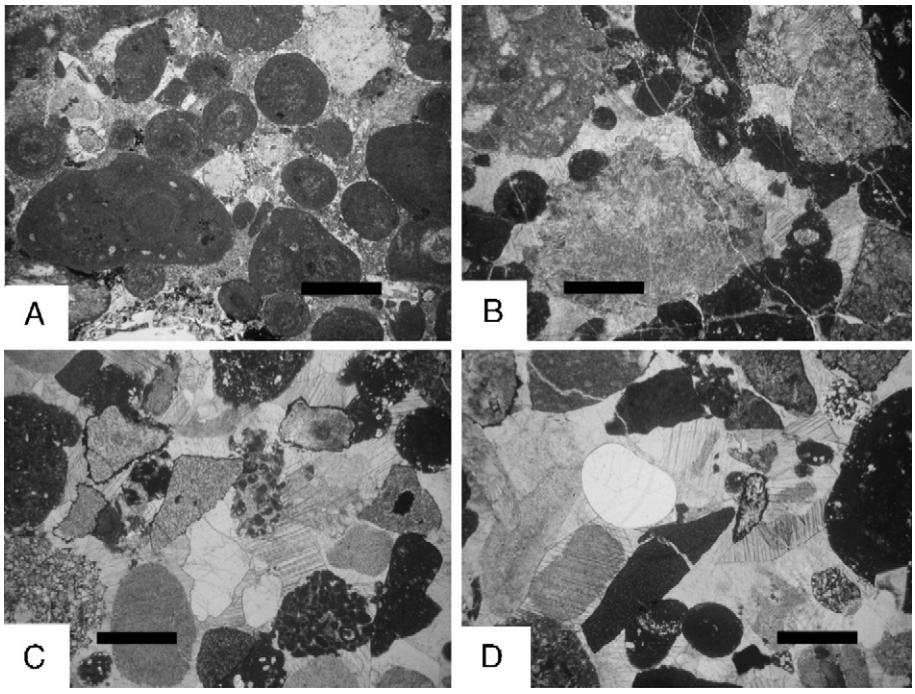

Fig. 10. Thin sections of conglomerate matrices: all plane polarized light. Scale bar is 1.0 mm. (A) Ooidal–grapestone–intraclast grainstone (conglomerate #3, M'aidan, loc. 7). (B) Overcompacted poorly sorted ooidal–intraclast–peloidal grainstone (lowermost conglomerate, Hammat Qusayd, loc. 1). (C) Compacted ooidal–bioclast–intraclast grainstone (uppermost conglomerate, Hammat Qusayd, loc. 1), bioclasts are dominated by echinoderm pieces. (D) Ooidal–bioclast–intraclast grainstone (uppermost conglomerate, Hammat Qusayd, loc. 1), with coarse well-rounded aeolian quartz sand grain and syntaxial overgrowths on echinoderm grains.

boulders, some from isolated carbonate platforms. The frequent three successively finer grained conglomerate to shale units within the horizon indicate three major progressively less intense depositional events separated by calmer periods.

The large lateral dimensions of the sheet-like, graded conglomerates indicate a source perpendicular to the flow direction and a poorly developed system of sediment distribution and the absence of definable channels and depositional lobes (Cooper, 1990). Though Cooper (1989) attributed the lack of definable channels and lobes to long transport across gentle slopes, most coarse submarine fans (and models derived from them) have channels and show channel switching and depositional lobes caused by rapid, short distance transport of coarse material down steep slopes (Walker, 1992). And pebbly turbidites require steep slopes to form (Nemec, 1990; Shanmugam and Moiola, 1991; Lee et al., 2002).

Extensive thick submarine conglomerates in finer grained turbidite successions are called megabreccias (megaturbidites), and have been attributed to catastrophic mass flows, perhaps triggered by earthquakes (seismoturbidites) (Mutti et al., 1984). Spence and Tucker (1997) attributed megabreccia formation to trapped overpressured pore waters during lowered sea-level allowing slope failure on even gentle slopes: but as they themselves noted there are few recent examples and inferences are made from ancient megabreccias. In addition, unless the sea-level dropped below the shelf edge then isostatic loading would be reduced and failure less likely at the shelf edge during regressions, though shelf margin breccia accumulation would be enhanced. Failure would be more likely during differential isostatic transgressional loading.

In the Bahamas, carbonate aprons rather than fans, are found along the deep flanks of the carbonate platforms (Mullins and Cook, 1986). The major difference between fans and aprons is a point source (or sources) with channelized sedimentation (as for the bulk of the Oolitic Limestone Member) and a line source with debris flow, grain flow and sheet flow sediments on aprons (as for the top conglomeratic horizon) (Mullins and Van Buren, 1979). The aprons change from proximal mud-supported ungraded megabreccias through clast-supported conglomerates and pebbly calcarenites to distal calcarenites and mudstones. The megabreccias occur as widespread sheets that may

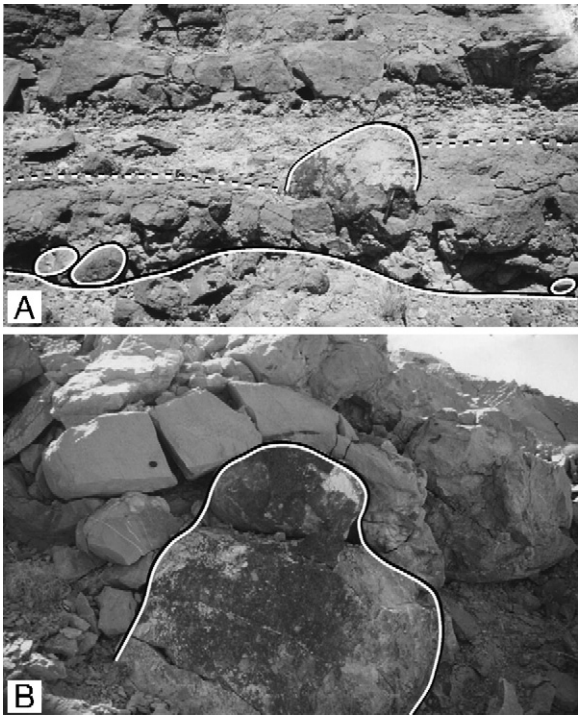

Fig. 11. Large clasts in conglomerates: (A) large rounded Triassic carbonate clasts with largest at top of coarser conglomerate (conglomerate #1, loc. 5, Sidr). (B) Chaotic texture in upper part of debris flow megabreccia, with large Triassic block overlain by fractured oolitic grainstone (conglomerate #1, loc. 10, Hubat).

exceed 25 m in thickness with hummocky upper surfaces capped by normally graded calcarenites (Mullins and Cook, 1986). These megabreccias and associated facies appear to represent major, episodic collapse events along bank or reef margins (Mullins et al., 1986).

The top Guwayza conglomerates have most of the characteristic of such deposits in that:

1) They are not organized in facies associations resulting from long-lived channel-lobe turbidite systems. The megabreccias form blankets extending across underlying fan facies boundaries (Fig. 4).
2) They comprise distinct sheet-like deposits that are easily recognizable and mappable. The top Guwayza conglomerates occur at an apparently constant stratigraphic horizon from the southern to the northern Oman mountains, and in the southern Oman mountains change from proximal megabreccias marginal to Saih Hatat through very coarse megabreccias at Sufra and Hubat to graded conglomerate–sandstone units in the basin, a distance of over 200 km (Fig. 3).
3) They have individual volumes and thicknesses one or two orders of magnitude larger than the thickest associated turbidites. The minimum total area of the top Guwayza conglomerates is 40,000 km^2, based on Cooper's (1990) reconstruction. Taking the minimum thickness of 2 m for the lowermost conglomeratic unit at M'aidan (Fig. 7, loc. 7), gives a minimum volume of 80 km^3 for that layer. The three conglomerates together (total thickness 6 m) have a minimum total volume of 240 km^3. In the Bahamas, Crevello and Schlager (1980) reported a spectacular carbonate debris sheet from Exuma Sound that covers the entire basin floor (~ 5400 km^2) with a volume in excess of 1.8 km3 and which traveled up to 120 km across the basin. It included muddy rubble from debris flow and conglomeratic grainstones from grain flows and graded grainstones from turbidity currents. Apart from the volume it closely resembles the top Guwayza conglomerates in facies and facies distributions. Some ancient megabreccias have volumes of up to 100 km^3 akin to those of the

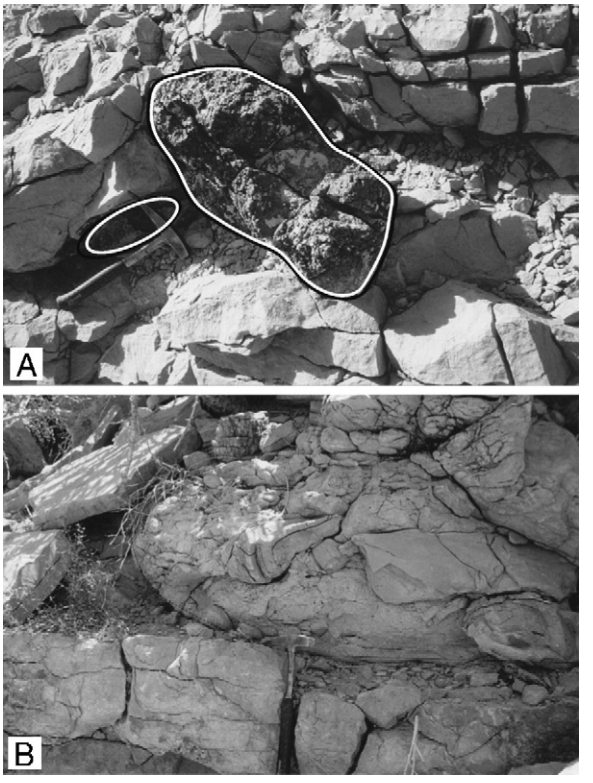

Fig. 12. Isolated clasts in conglomerates. Hammer is 30 cm long. (A) Amygdaloidal basalt boulders (outlined), erupted subaerially or in shallow water. (B) Distorted slumped slope limestone slump in conglomerate (both loc. 9, Sufra).

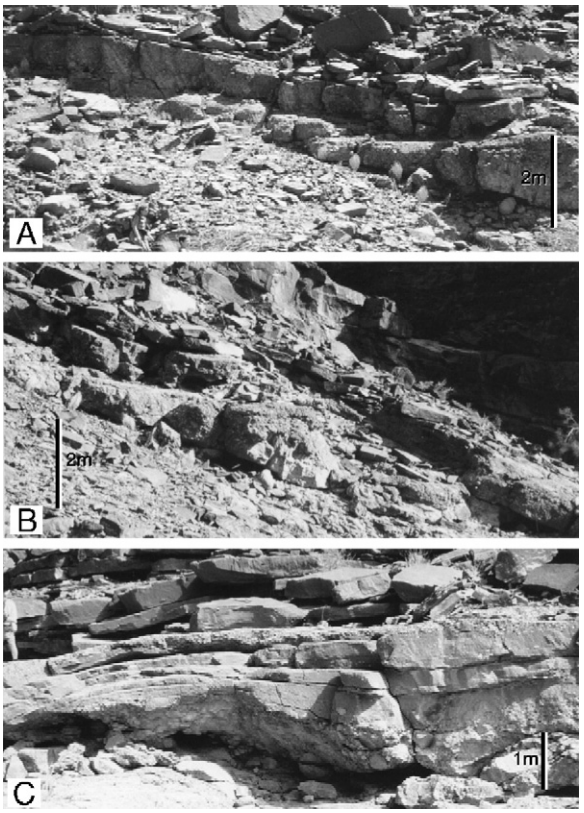

Fig. 13. Long wavelength hummocky cross-bedding (A), divergent cross-stratification (B) and multiple units (C) in graded conglomerates (all conglomerate #1, loc. 7, M'aidan). Left part of (B) overlaps right part of (A).

top Guwayza conglomerates (Mutti et al., 1984). These are almost exact analogues for the top Guwayza conglomerates, which also fit the ideal 'megaturbidite' profile of Mutti et al. (1984, their Fig. 1).

4) They include distorted clasts of slope facies concentrated at the tops of the breccia units (Mutti et al., 1984), as do the top Guwayza conglomerates (Fig. 11B).

The top Guwayza conglomerates do not have one characteristic of such deposits—occurrence as random intercalations within and across basin plain and deep-sea fan sequences (Mutti et al., 1984). The top Guwayza conglomerates mark a major sedimentary change from the carbonate submarine fan of the Oolitic Limestone Member to the pelagic deep-water carbonate/chert sediments of the Sidr Formation (Fig. 5) (Blechschmidt et al., 2004). The divergent current directions and hummocky cross-stratification shown both in the conglomerates and sandstones could be produced by a number of processes, including: a) sediment waves and large blocks on the initial slump surfaces producing antidunes and resulting antidune cross-stratification; b) divergent currents caused by deflection by obstructions on and adjacent to the fan; and c) exceptionally deep wave action.

(a) Coarse-grained deep water sediment waves are common on the levees of submarine channels of steep submarine fans (Wynn and Stow, 2002) and have been interpreted as large antidunes produced by turbidity currents, the main reason for this interpretation being the upstream migration of their internal layering (Nemec, 1990). The upstream migration is a result of differential deposition between both sides of the waves, with the upstream side migrating (usually very rapidly) against current flow during antidune development (Kennedy, 1969). However, coarse-grained turbidites are restricted to channels and channel–lobe transitions (Wynn et al., 2000). Furthermore, antidunes form at supercritical Froude numbers (>1) where turbidity currents are erosional and upstream deposition only occurs with rapidly migrating antidunes close to the critical Froude number hydraulic jump (Allen, 1982). Lastly, appropriate velocities can only be generated on steep slopes, though it has been suggested that acceleration back to supercritical after a hydraulic jump (perhaps after an obstacle) may produce a succession of antidune sediment waves downflow (Van den Berg et al., 2002). In any case, rare cross-sections through coarse-grained sediment waves show clear evidence of down-current migration in a manner typical of dunes rather than antidunes (Piper and Kontoupolis, 1994). Only large fine-grained sediment waves look similar to slope failure deposits but the former have well-organized internal layering with upslope migrating mega cross-lamination (Lee et al., 2002). Antidunes can also be produced by obstructions such as large blocks or corrugations in mass flows causing deceleration followed by acceleration to supercitical after the obstruction. In this case the antidunes are generated by obstructions in the flow rather than being caused by supercritical flow. However, even in this case, experiments have shown that deposition occurs when flow conditions are outside the stability field for antidunes (Kubo, 2002).

Applying all this to the top Guwayza conglomerates, the downflow dipping cross-bedded conglomerates (Fig. 13B) could be caused by subcritical flow forming bars on top of the mass flow conglomerates below, followed by antidune formation with increased flow velocities and the formation of the low angle upstream dipping cross-bedded conglomerates to their

left (Fig. 13A). However, continual decreasing flow velocity is shown by the equally divergently dipping hummocky cross beds of the overlying grainstones (Fig. 13C) which should be formed during lower subcritical current velocities incapable of forming antidunes. Obstructions to flow certainly occur in the more proximal megabreccias of the top Guwayza conglomerates (Fig. 11), but there are no such obstructions in the more distal conglomerates we studied at M'aidan (Fig. 13).

(b) Ancient turbidites with divergent flow directions (indicated by divergent cross-laminations) are often called 'contained turbidites' and supposedly caused by deflected and reflected turbidity current flow paths around and from sea-floor irregularities (Pickering and Hiscott, 1985; Cooper, 1989). Most 'contained turbidites' have been described from ancient inferred tectonically active basins where any obstructions have to be inferred: and often such obstructions are supposed to be submarine fan levees or fault blocks (Haughton, 2001; Felletti, 2002). But, simple deflection by obstacles is insufficient to form reversed current directions. Actual reversals of turbidity currents have experimentally been shown to be only possible when the current runs up a slope and then falls back; or with two distinct turbidity currents coming from different directions (Edwards, 1993). On the Guwayza fan, swamped by the top Guwayza mass flows, the only contemporary topography capable of reflecting and reversing turbidity currents are the Oman exotics which, from reconstructions, were over 200 km from the most distal sections across an abyssal plain (Fig. 3).

(c) Divergent flow directions in the same bed can be caused by interfering wave systems, though the problem is that most of the top Guwayza conglomeratic facies are coarse and deepwater and associated with slumps

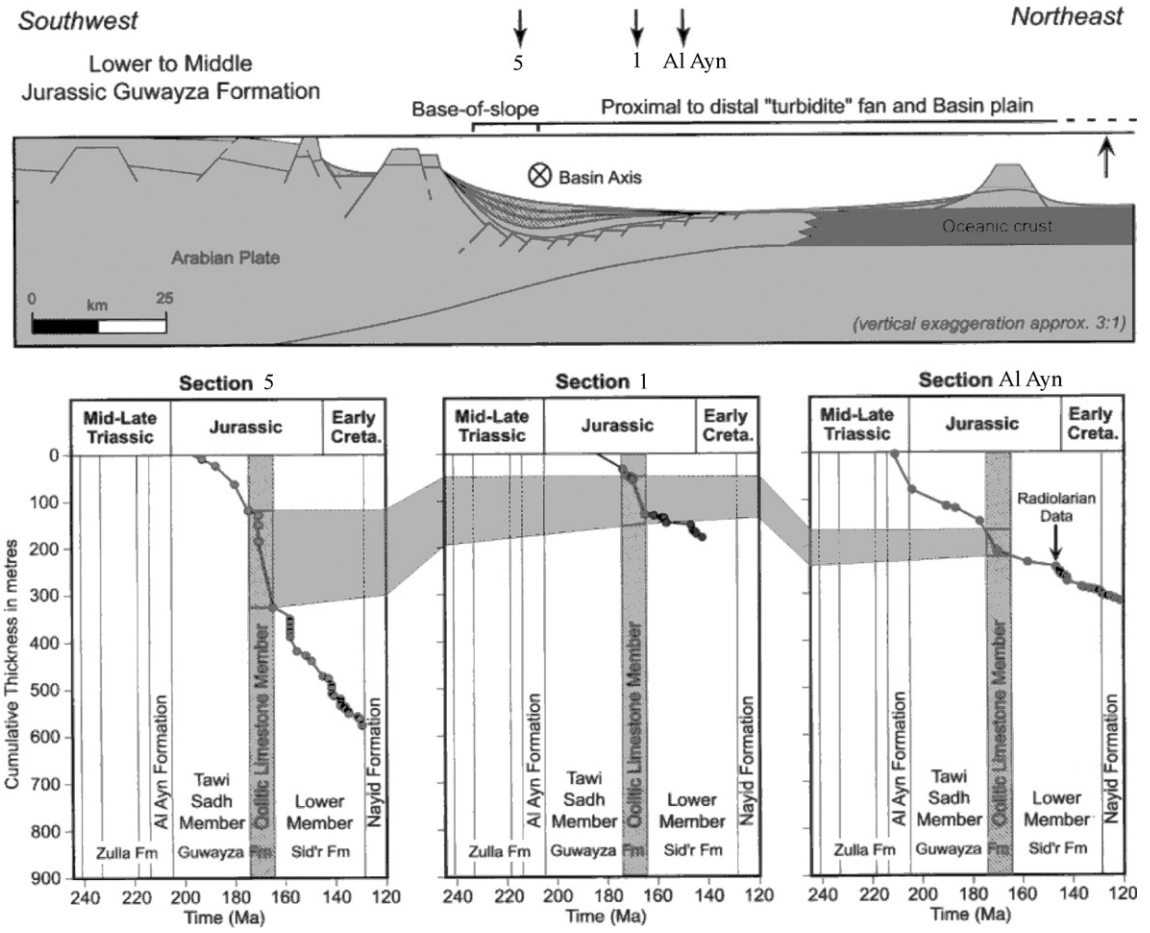

Fig. 14. (A) Cross-section of block-faulted Oman passive margin during deposition of the Oolitic Limestone Member in the Hamrat Ad Duru basin. (B) Accumulation curves of three section including the Oolitic Limestone Member (without decompaction). Note that accumulation/subsidence rates are highest for the Oolitic Limestone Member and especially at the base of slope.

(megabreccias). Nevertheless, hummocky cross-stratification in shallow water is almost always attributed to variable oscillatory flows caused by interfering waves, not successive divergent currents which would give separate cross-stratified beds (Duke et al., 1991). Hummocky cross-stratification in ancient turbidites has been attributed to deposition in relatively shallow water (e.g. Myrow et al., 2002), but this need not necessarily be the case if the waves are large enough. We consider that the hummocky cross-stratified beds in the top Guwayza conglomerates and grainstones (which are gradational) were caused by oscillatory wave action in deep water. In that case velocities of >5 m s^{-1} would be needed at the sea-floor to move the mean 5 cm diameter clasts in the upper parts of the conglomerates (larger clasts could move on these like ball bearings) (Allen, 1982).

Such velocities deposit shelf storm layers when nearshore material is remobilized by onshore storm waves and transported offshore by strong bottom surge currents, to be redistributed in graded hummocky cross-stratified beds by progressively weaker waves (Seilacher and Aigner, 1991; Myrow and Southard, 1996). However, the top Oolitic Limestone Member conglomerates and grainstones were deposited off a passive margin, in places at least 1000 m below sea-level at the base of a carbonate fan (Cooper, 1990), during a period of rapid tectonic subsidence at the base of slope (Fig. 14) (Blechschmidt et al., 2004). For waves to move or rework such coarse sediment at such depths requires very large waves.

Order of magnitude estimates for wave height and period can be obtained from the threshold velocities required to move various sized grains in waters of specific depths (Fig. 15). For example, to move the mean 1–2 mm diameter very coarse sand matrix of the conglomerates and grainstones (threshold for movement about 1 m s^{-1}) at a depth of 1 km (a minimum depth for the distal part of the Oman passive margin fan—see Cooper, 1990) requires open ocean waves over 10 m high at waves periods of over 1000 s, increasing with decreasing wave period to over 500 m high at 25 s (Fig. 15). Far larger waves would be required to move the larger pebbles and boulders in the top Guwayza conglomerates any distance at such depths.

Waves 10 m high are near the limit of normal storm and hurricane waves and surges, but these (and larger waves) are possible with large tsunami (NOAA: Saffir–Simpson Hurricane Scale). The characteristics of the top Oolitic Limestone Member conglomerates are very similar, though thinner, to the only well-described coarse, wave reworked, inferred deep-water giant

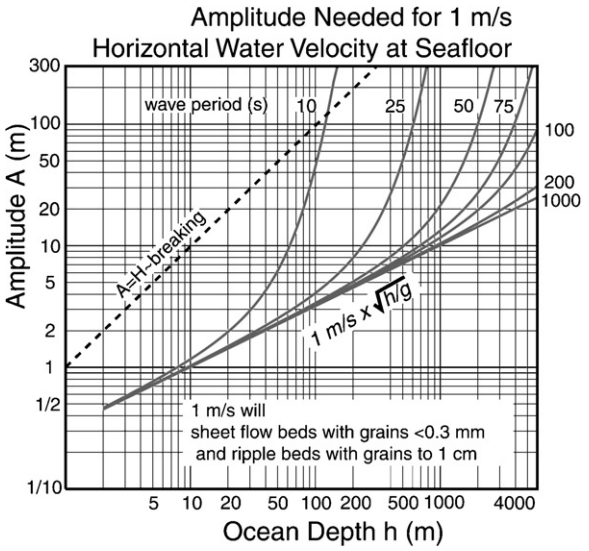

Fig. 15. Graph of wave amplitudes required for velocities of 1 m s^{-1} at the sea floor (capable of moving grains to 1 cm diameter) plotted against ocean depth. Diagram courtesy of Simon Ward.

tsunami deposits so far recorded in the stratigraphic record—those related to the end Cretaceous impact-generated tsunamis in the Caribbean (Takayama et al., 2000; Tada et al., 2002). Tsunami, however, can be generated in a number of ways.

4. Generation of large tsunamis

Tsunami are generated by any non-meteorological displacement of the surface of a water body. Tsunami of the order of metres in amplitude are relatively common in all oceans, and as many as 50 large tsunami deposits (>5 m runup height) are preserved on the Pacific coast of Kamchatka over the last 7000 years (Pinegina et al., 2003); approximately one every hundred years. Coastal and shallow-water tsunami deposits should thus be common in the stratigraphic record (Coleman, 1968; Bryant, 2001), but very few have been described (e.g. Takashimizu and Masuda, 2000; Pratt, 2002) even though Klein and Marsaglia (1987) considered that some hummocky beds could be generated by tsunami rather than by storm waves. One upper bathyal tsunami deposit has been described from the Miocene of Japan (Shiki and Yamazaki, 1996). However, tsunami capable of affecting deep shelf and oceanic sea-floors need to be of very large amplitude and wavelength since wave motion extends only to a depth of about one-half the wavelength, and lateral motion is dependent on the wave amplitude. Most open ocean tsunami waves have the required wavelengths (up to 100 km or so) but not

the amplitude (a few metres maximum) to significantly move sediment in deep water (Yeats et al., 1997).

Giant tsunami up to several hundred or more metres are required for waves to move sediment in deep water. Fault displacements and explosive submarine eruptions can generate large tsunami (to dekametre scale). Fault displacements generate only moderate tsunami, since an instantaneous 10-m vertical fault displacement during a great earthquake cannot initially generate higher tsunami waves, though they often do trigger large slides (Ben-Menahem and Rosenman, 1972; Dawson, 1999). Even large submarine eruptions only generate deka-scale tsunami. The great submarine Krakatau explosion (1883) triggered tsunami only a metre or so high in open water, though locally 30 m high in shallow water (Winchester, 2003). On 13th March, 1888, 5 km^3 of the Ritter Island volcano, northeast of Papua New Guinea, fell into the sea. This event, the largest lateral collapse of a volcanic island in historic times generated devastating tsunami which were, however, only a few tens of metres high (Silver et al., 2005).

Only oceanic meteorite impacts and submarine landslides can potentially generate larger tsunami, hundreds or even thousands of metres in height in the open ocean (Trifunac and Todorovska, 2002; McMurtry et al., 2004).

Large meteorite impacts into oceans can immediately displace the entire water column and generate tsunami initially higher than the depth of the ocean. A large kilometre-sized asteroid impacting a deep ocean generates initial tsunami waves of comparable height to the ocean depths, and these, despite attenuation, would still be more than 100 m high when they reached the surrounding coasts (Hills and Mader, 1997). The Eltanin asteroid impact (around 1–4 km diameter) impacted the south Pacific in the late Pliocene (around 2.15 Ma) depositing ejecta and reworking deep-marine sediments into distinctive beds which can be used to characterize such deposits (Gersonde et al., 1997); though the only described coastal record of it is in Chile (Hartley et al., 2001). Impact tsunami are relatively rare events though their deposits should be at least sporadically found in the stratigraphic record. In contrast, very large slides from oceanic islands and continental margins are much commoner (Carracedo et al., 1999; Tinti and Bortolucci, 2000; Ward, 2001). Slide-generated tsunami deposits should thus be a normal and common feature in the stratigraphic record (Watts, 2003).

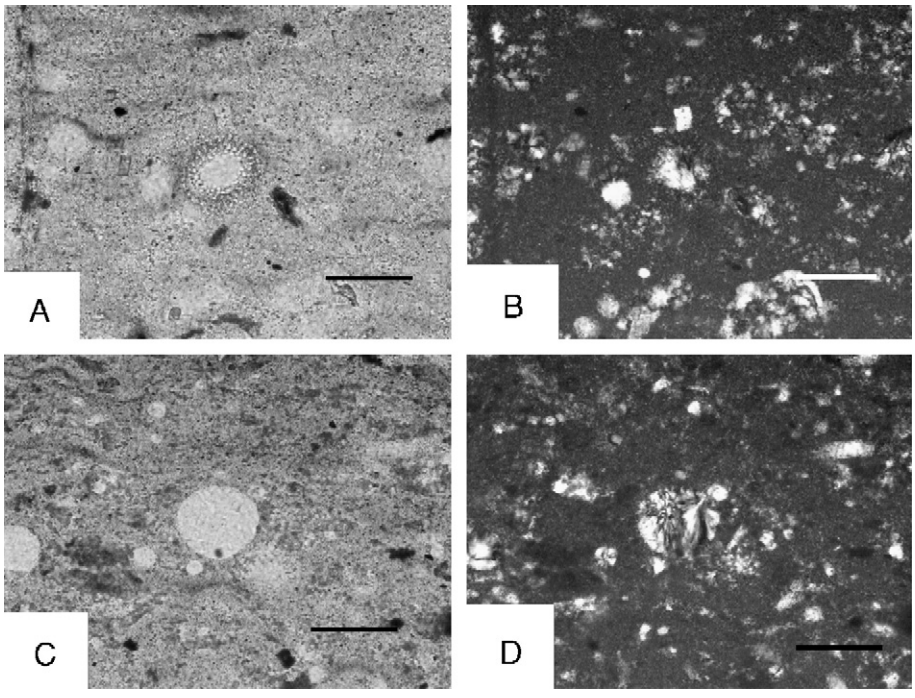

Fig. 16. Thin sections of spherules in green clay above topmost conglomerates at M'aidin. Scale bar is 100 μm. (A) Plane polarized light. Central spherule has geometric mesh texture and chloritic rim; probably recrystallized and replaced radiolarian. (B) Same as A, crossed nicols. Central spherule shows central fill of radial-fibrous chalcedony. (C) Plane polarized light. Central spherule has no chloritic rim and consists entirely of chalcedony. (D) Same as C, crossed nicols. Central spherule showing several radial-fibrous chalcedony fans: most probably altered radiolarian; smaller spherules may be younger ontogenetic stages.

Submarine landslides can generate tsunami nearly as high as the initial displacement if the slide accelerates fast enough (Keating and McGuire, 2000; Ward, 2001, Todorovska et al., 2002). In Lituya Bay, Alaska, a landslide into the bay in 1958 generated an initial wave over 500 m high, which then rapidly dissipated to tens of metres down the 12 km long bay where it sank several fishing boats (Pararas-Carayannis, 1999; Fritz et al., 2001). In 1929, a magnitude 7.2 earthquake triggered a huge submarine slump (200 km^3) on the Grand Banks of Newfoundland which, in turn, generated a tsunami which reached amplitudes of 2 to 7 m along the Newfoundland coast, deposited a 5 cm layer of sand over coastal peats, and killed 27 people in the worst tsunami disaster in Canadian history (Bornhold et al., 2003). Dozens of major submarine landslides have been discovered on the flanks of the Hawaiian ridges and are among the largest on Earth, with lengths greater than 200 km and volumes of 5000 km^3 (Moore et al., 1994). These huge Quaternary submarine landslides, and similar slides around the Canary islands may have generated large tsunamis, though so far the evidence is disputed (Felton et al., 2000; Rubin et al., 2000; Keating and Helsey, 2002; McMurtry et al., 2004; personal observations in coastal Mauritania in 2004). However, the Quaternary second Storegga slide (1700 km^3; 7000 B.P.) off Norway has been considered the trigger for a tsunami which deposited widespread subaerial sands in Norway and eastern Scotland (Bondevik et al., 1997).

But, were the tsunami that reworked the top Oolitic Limestone Member conglomerates triggered by impact, volcanic eruption, faulting, or slope failure? The massive Jurassic submarine breccias recorded in many of the Oman shelf margin deposits (as noted above) suggest submarine slope failures. However, it is still worthwhile looking at the petrology and geochemistry of the conglomerates and overlying sediments for evidence of the other possible causes.

Table 1
Major element analyses of whole rock samples

Oxides in wt.%	OMAN 1	OMAN 2	OMAN 3	OMAN 4	OMAN 5
SiO_2	83.71	30.39	63.69	72.22	71.14
Al_2O_3	3.65	0.66	2.29	1.95	10.51
Fe_2O_3	3.74	0.82	2.21	2.29	5.73
FeO	3.37	0.74	1.99	2.06	5.16
MnO	0.014	0.032	0.023	0.011	0.006
MgO	2.19	0.84	1.09	0.66	2.86
CaO	1.78	37.05	15.49	0.77	0.71
Na_2O	0.23	0.04	0.16	0.19	0.66
K_2O	0.62	0.08	0.51	0.36	3.12
TiO_2	0.3	0.104	0.269	0.164	0.788
P_2O_5	0.07	0.05	0.269	0.1	0.22
LOI	3.16	29.91	14.04	1.38	4.53

Table 2
Trace element analyses (ppm) of samples as in Table 1: detection limits range from 5 to 20 ppb except Au and Ir at 2 ppb

Concentration (ppm)	OMAN 1	OMAN 2	OMAN 3	OMAN 4	OMAN 5
Au	3000	4000			
As	1			1	
Br		0.8	0.6	0.8	
Co	6	1.7	2.3	3.3	9
Cr	26.7	10.9	20.8	21	65.3
Cs	3.4	0.5	2.6	1.4	16.3
Hf	1.6	4.1	3.7	2.7	4.2
Hg					
Ir					
Mo	3				
Rb	21		19	14	121
Sb	0.2		0.1	0.2	0.4
Sc	4	3.6	5.7	2.1	13.8
Se					0.8
Ta			0.4	0.4	0.9
Th	3.3	1.5	3	3.1	10.5
U	0.4	0.8	0.8	0.5	0.9
W					2
La	9	15.6	13.7	8.4	23.3
Ce	18	23	25	18	46
Nd	9	11	14	10	25
Sm	2.02	1.99	3.15	2.24	5.29
Eu	0.51	0.51	0.78	0.58	1.24
Tb	0.3	0.3	0.5	0.3	0.6
Yb	0.66	1.28	1.27	0.73	1.71
Lu	0.1	0.2	0.18	0.11	0.25
Cd	0.3				
Cu	34	8	23	37	43
Ni	21	3	20	14	41
Pb	8	4	9	5	9
Zn	58	20	29	25	79
S%	0.018	0.048	0.021	0.25	0.13
Ba	97	14	30	255	89
Sr	63	185	102	71	90
Y	10	15	19	10	21
Zr	65	151	157	107	157
Be					1
V	29	10	20	15	82

5. Petrology

The conglomerates and sands contain no identifiable impact melt or intermediate to acid volcanic clasts. The minor quartz sand has no impact deformation lamellae and none of the euhedral faces of fresh volcanic quartz, but contain rutile and tourmaline typical of a plutonic/high grade metamorphic source.

The cherts in the fine-grained units above the conglomerates contain small greenish circular bodies

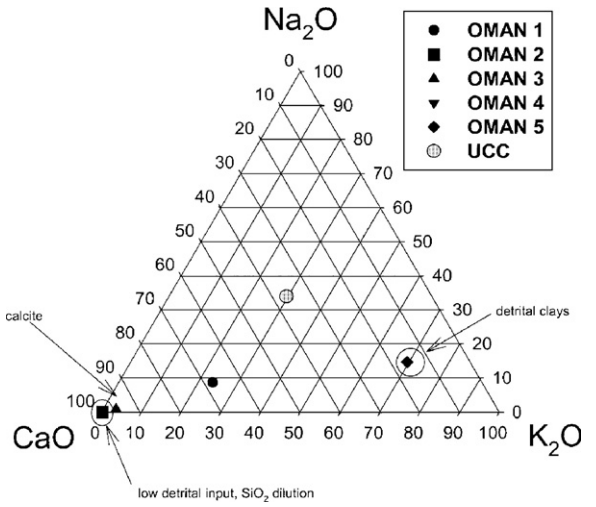

Fig. 17. Alkali–Alkali Earth chemistry of whole rock sediments. Upper continental crust (UCC) is shown for comparison (Condie, 1993). Sample description (all from 30 cm Green shale/chert unit above topmost conglomerate, at junction with Sidr Formation). OMAN 1: Medium dark grey (4N4) laminated silty, cherty mudstone, 1 cm thick, with 10% small rounded dominantly chalcedony spherules around 100 μm diameter. OMAN 2: Medium grey (5N5) sandy peloidal grainstone (limestone), 2 cm thick, with scattered angular to rounded quartz sand (5–20%) in a matrix of peloidal sparite cement with a few scattered small dolomitic extraclasts. No multiple shock lamellae in quartz sand. OMAN 3: Medium grey (5N5) calcareous very fine quartz sandstone and sandy peloidal grainstone (limestone) with rare chalcedony spherules and abundant small dolomitic extraclasts. No multiple shock lamellae in quartz. OMAN 4: Medium grey (5N5) laminated silty (?) recrystallized chert with abundant chalcedony spherules (similar to OMAN 1). OMAN 5: Greenish silty shale.

about 100 μm in diameter (Fig. 16). But these have neither the internal vesicles and cracks found in impact spherules, nor the oval or irregular cross-sections indicating the teardrop and dumbell shapes of once molten material. Their radial-fibrous chalcedony fillings are more like void-filling precipitates than devitrified impact spherules, since the fillings consists of only one to several fans. Devitrified impact spherules usually show a large number of inwardly directed botryoidal fans, and generally have authigenic felspar and/or more exotic silicates in addition to the chalcedony (Simonson and Glass, 2004). Furthermore, a minority of the circular bodies have clear isopachous rings around their edges, and geometric mesh textures via intergrowths of a second phase (?) chloritic mineral, which do not occur in impact spherules, but may be replaced shell material. Lastly, the circular bodies do not form a hydrodynamically compatible detrital framework as tsunami-reworked impact spherules do. They are rather homogeneously mixed with the finer-grained sediment, as if they settled out from pelagic suspensions, and are almost certainly altered radiolaria (Paulian Dumitrica, pers. comm.).

6. Geochemistry

Geochemical methods used and sample descriptions are in Appendix A. Because of the problem of dilution in the shallow-water derived carbonate sands and gravels, major and minor element and REE analyses were done only on the finer cherts, limestones and shales in the 30 cm thick unit above the uppermost conglomerate (Fig. 8B; Tables 1 and 2). These finer grained, post-mass flow sediments are most likely to show the geochemical signature of the processes which may have generated the mass flows and the waves which reworked them.

The major element geochemistry of the fine-grained sediments provides insights into both the provenance of these sediments as well as their diagenetic history. Based on the petrography of these samples there is significant diagenetic replacement by calcite. Major element variations show relatively low concentrations of CaO relative to average shale and continental crust and high SiO_2 concentrations typical of fine-grained sands and cherts (Figs. 17 and 18). The fine-grained cherts contain minor amounts of alkali metals and are rich in CaO compared to Upper Continental Crust (UCC) (Condie, 1993). The variations in silica, calcium, magnesium and aluminum oxides point to a common chemistry for the bulk samples suggesting a common depositional, diagenetic and provenance history. The high silica content of the whole-rocks may dilute the provenance

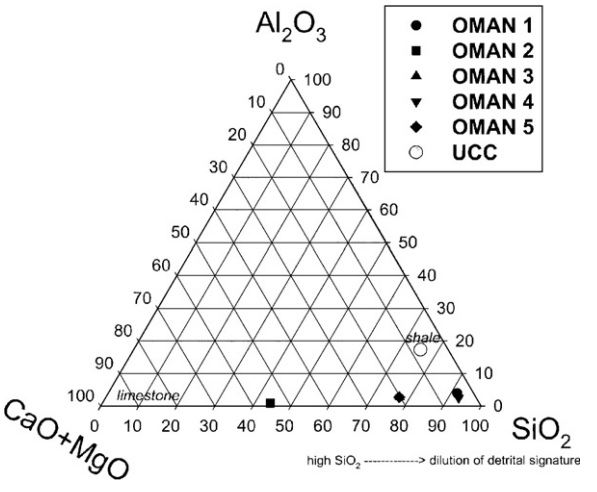

Fig. 18. Variations in Al_2O_3, CaO + MgO, SiO_2: with fields for average limestone and shale (Taylor and McLennan, 1985).

signatures (though this dilution effect can be, to some degree, alleviated by the use of LA-ICP-MS). Despite the dilution effect of SiO_2 the major element geochemistry records detrital signatures and hence information concerning the provenance of these sediments. SiO_2/Al_2O_3 and Al_2O3/TiO_2 ratios are all greater than 20 suggesting a significant detrital component and that at least some of the fine-grained silica is allochthonous (Fig. 19) (Franceschelli et al., 1996).

Given that there is a significant detrital component in the Oman sediments we explored the provenance of these sediments using the trace element signatures of the bulk rock and lasered material. Although the bulk samples show chemistries characteristic of their provenance the LA-ICP-MS provide more detail concerning both the provenance and early diagenetic history of the sediments. Trace element and REE abundance patterns are useful provenance indicators in fresh, unweathered sedimentary rocks (Taylor and McLennan, 1985; Hannigan and Basu, 1998 and references therein). We

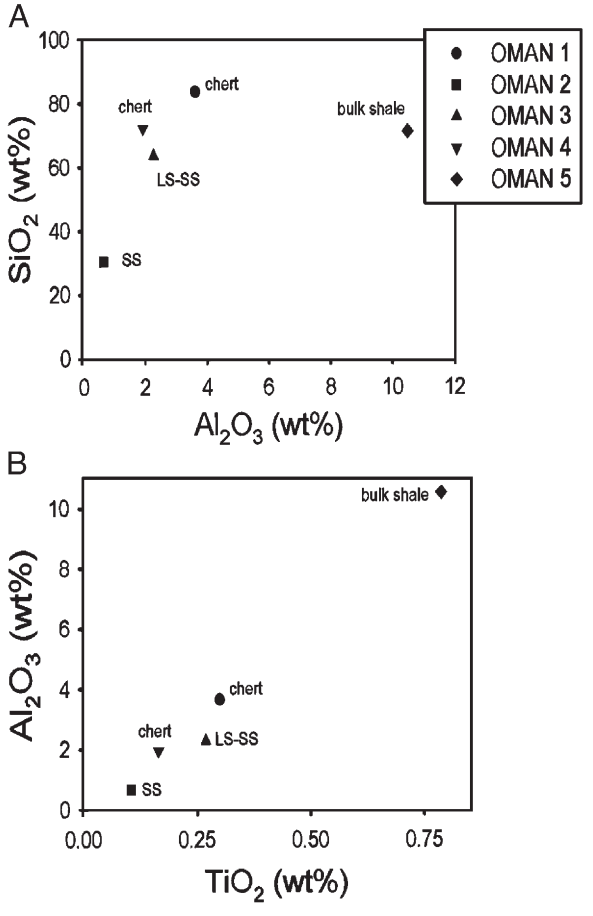

Fig. 19. (A) SiO_2/Al_2O_3 plot; (B) Al_2O_3/TiO_2 plot. LS-SS is sandy limestone, SS is sandstone.

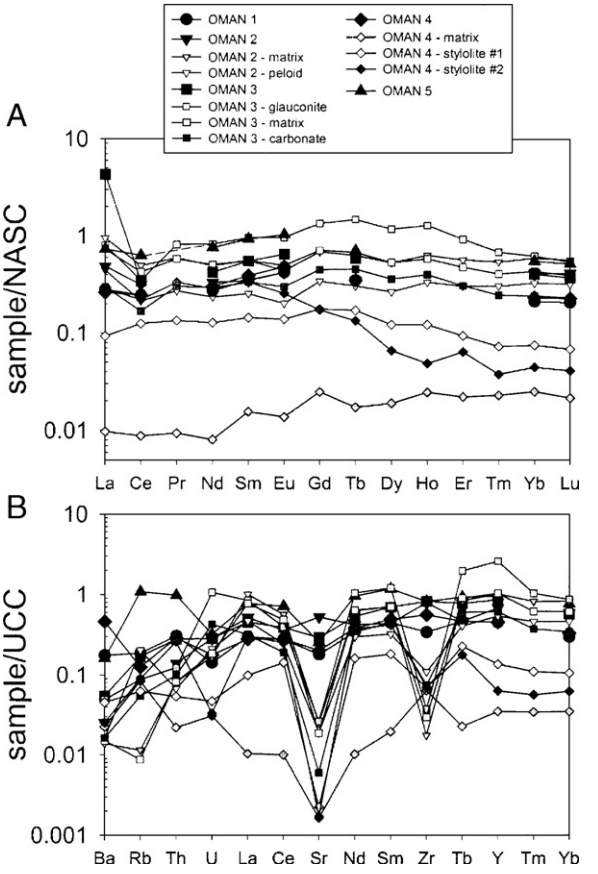

Fig. 20. (A) NASC-normalized REE composition of bulk analyses and lasered material; (B) UCC-normalized trace element abundances of bulk analyses and lasered material.

compare the trace element and rare earth element (REE) abundance patterns of the Oman sediments to average shale (NASC) and upper continental crust (UCC) (Fig. 20). Although the fine-grained sandstones and cherts (OMAN 1 and 4) have the lowest overall REE abundances, all five bulk sediments show the same abundance pattern relative to average shale suggesting a common provenance. The NASC-normalized patterns of the bulk sediments (Fig. 20A) show slight middle REE enrichments (MREE) similar to chert-phosphorite patterns including Ce depletion (Mazumdar et al., 1999). Trace element abundances in the samples normalized to upper continental crust also show typical sediment patterns (Fig. 20B). The only dramatic difference between samples is the variation in Rb and Sr concentrations, which is attributable to variable amounts of carbonate and siliciclastic material. However, selective analysis of individual components by LA-ICP-MS can isolate the detrital fraction components as shown in Fig. 20.

The relationships between shale-normalized La and Ce to Al_2O_3 and Fe_2O_3 also provide some insight into the depositional setting and provenance of the sediments (Fig. 21) (Murray, 1994). Here, the bulk sediment chemistry appears to be a mixture of pelagic and continental margin material and this mixed signature supports rapid sedimentation in or near a continental margin setting. Curiously, only the peloidal grainstone (OMAN 2) plots well within the pelagic field, suggesting the peloids are the excrement of planktonic organisms.

The cherts and grainstone (OMAN 1–4) are interbedded within a green shale (OMAN 5). It is possible, by comparing the elemental signatures of the cherts to the shale, to estimate the amount of terrigenous material accumulated in the fine-grained cherts (Fig. 22). The REE-normalized patterns of the cherts when compared to the bulk green shale (OMAN 5) show remarkable consistency in patterns and provide further evidence of a common mixed continental margin/pelagic provenance for the detrital fraction (Fig. 22A). The relative depletion in light REE suggests deposition under relatively oxidized conditions with the fractionation of light REE likely due to dilution effects of carbonate which is depleted in light REE. Although the relative abundances of the REE in the cherts and lasered fractions show a relatively flat pattern, several trace elements are significantly fractionated from the bulk shale pattern (Fig. 22B).

As discussed above the variations in Sr and Rb are easily explained by the relative abundance of carbonate in the sample and as expected the lasered chert material has significantly less Sr than the bulk shale or stylolite samples. The bulk samples show higher amounts of Zr,

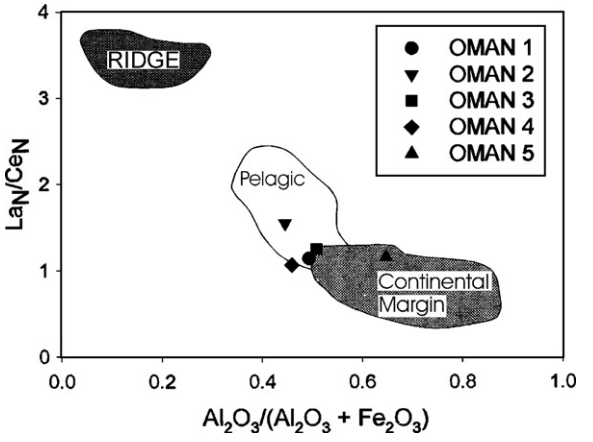

Fig. 21. La/Ce shale normalized ratios versus major oxide compositions for the bulk sediments. Fields for representative marine environments from Murray (1994).

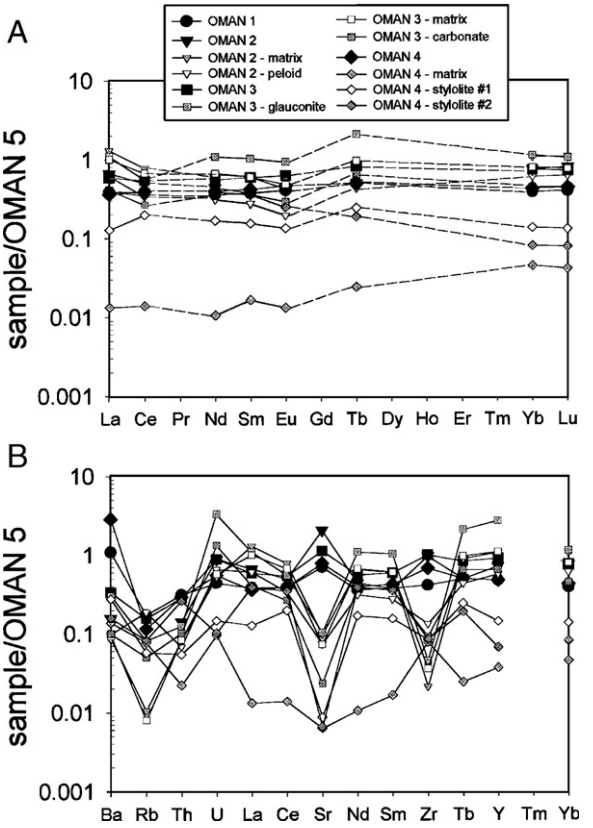

Fig. 22. Rare earth (A) and trace elements (B) of bulk analyses and lasered material normalized to the host shale (OMAN 5).

which is consistent with a higher amount of detrital material than in the lasered samples. The lasered glauconite has the expected high U values typical of an early diagenetic mineral.

The main conclusions from the geochemistry are that the cherts, limestone and shale samples all share a mixed pelagic–continental margin provenance and that chemical fractionation of the cherts relative to the bulk shale occurred during diagenesis rather than during sedimentation. The consistency of the provenance patterns and trace element abundances suggests that sedimentation of these cherts was relatively rapid; indeed it had to be to allow for the terrestrial detritus signature to be visible.

7. Clay mineral analysis

X-ray diffraction analyses (methods in Appendix A) of the green silty clay (OMAN 5) show a composition dominated by a clay mica (commonly referred to as illite) and quartz with minor amounts of kaolinite and no expanding clay minerals. The lack of expanding clay minerals is unusual in unmetamorphosed pelagic clays which are usually dominated by expanding clays

derived from weathered volcanic dust. This confirms the rapid continent-derived sedimentation suggested by the geochemistry.

8. Conclusions

We suggest that the top Guwayza conglomerates were initially deposited by mass flows generated by massive submarine slope failures during mid-Callovian normal faulting. Very large tsunami, perhaps hundreds of metres high, generated by the submarine slides, reworked the upper parts of the successive submarine slides. In the absence of evidence for impact or volcanic activity associated with the conglomerates, or the overlying clays and cherts, tsunami associated with either earthquakes or mass flows (submarine slides) are the preferred agent of deposition of the top Guwayza conglomerates. Since even very great earthquakes generate only 'moderate' tsunami up to dekametres in height, we tentatively conclude that the main agent that triggered the tsunami were enormous submarine mass flows analogous to those around the Hawaiian and Canary Islands. There is little evidence for submarine sliding or megabreccia formation around the oceanic seamounts during the mid-Jurassic, though there is evidence for non-deposition and erosion on their deep-water surfaces (Béchennec et al., 1988). However, there is evidence for large-scale passive margin subsidence and mega-breccia formation on the Saih Hatat block around the time of deposition of the top Guwayza conglomerates. The Guwayza triple conglomerate horizon suggests repeated generation of tsunami and mass flows deposited conglomerates along and against the Jebel Akhdar/Saih Hatat fault during subsidence. But what triggered this subsidence?

The Callovian stage marks one of the greatest marine transgressions of the Jurassic (Hallam, 2001) and the Middle to Late Callovian is the time of maximum flooding over the Arabian platform during the Jurassic (Le Nindre et al., 2003). The consequent water-loading of the shelf may have triggered major continental slope failures on the Tethyan passive margins (Dawson, 1999), especially since at least 200 m of basement subsidence occurred on the Arabian platform at the latitude of central Oman (Le Nindre et al., 2003). Deposition of the Oolitic Limestone Member ceased during the younger Oxfordian sea-level rise (with a return to more normal, slower, subsidence on the Arabian platform) which spread pelagic deposits of the Sidr Formation far across the Oman passive margin (Béchennec et al., 1988). The stacking of three similar but fining upward tsunami deposits at the top of the Oolitic Limestone Member, and the possibility that some of the graded conglomerates beneath and above are also tsunami deposits, suggest a repetitive non-impact mechanism.

Curiously, this study, which began with us considering a hypothesis of impact-generated tsunami as an explanation for the top Guwayza conglomerates, ends with a return to the older slope failure model of Cooper (1989), though tsunami were not then thought of. There may be evidence elsewhere around the adjacent contemporary Tethyan margins for at least subdued tsunami effects during the Jurassic, and we intend checking on this. Furthermore, many of the great megabreccias of the Triassic and Cretaceous in Oman have the same characteristics as those of the top Guwayza conglomerates (Robertson and Searle, 1990) and may also have tsunami deposits associated with them. Considering the frequency of tsunami in modern oceans, the surprise is not that palaeotsunami deposits occur, but that so few have so far been described.

Acknowledgments

Blechschmidt's work is partly supported by the Swiss National Foundation (project no. 2000-050681) at the University of Bern. Brookfield's work is supported by a research grant from N.S.E.R.C. Canada. We thank the Ministry of Commerce and Industry, Sultanate of Oman, especially its Director General, Dr. Hilal Al Azri, for logistic support during field work. We appreciate the comments on earlier versions of the manuscript by K. Crook and discussion and criticism by A. Matter.

Appendix A. Sample descriptions, and geochemical and clay mineral analytical methods

A.1. Sample description

OMAN 1. Medium dark grey (4N4) laminated silty, cherty mudstone, 1 cm thick, with 10% small rounded dominantly chalcedony spherules around 100 μm diameter.

OMAN 2. Medium grey (5N5) sandy peloidal grainstone (limestone), 2 cm thick, scattered angular to rounded quartz sand (5–20%) in a matrix of peloidal sparite cement with a few scattered small dolomitic extraclasts. No multiple shock lamellae in quartz grains.

OMAN 3. Medium grey (5N5) calcareous very fine quartz sandstone and sandy peloidal grainstone (limestone) with rare chalcedony spherules and abundant small dolomitic extraclasts. No multiple shock lamellae in quartz.

OMAN 4. Medium grey (5N5) laminated silty (?) recrystallized chert with abundant chalcedony spherules (similar to OMAN 1).

OMAN 5. Greenish silty shale.

A.2. Geochemical analysis

Major, minor and trace elements were analyzed with ICP-MS, INAA, and XRF by Activation Laboratories Ltd., who supplied the following text.

1) Inductively Coupled Plasma-Mass Spectometry (ICP-MS)

For major elements, a 0.2 g sample is mixed with a mixture of lithium metaborate/lithium tetraborate and fused in a graphite crucible. The molten mixture is poured into a 5% nitric acid solution and shaken until dissolved (~ 30 min). The samples are run for major oxides and selected traces on a combination simultaneous/sequential Thermo Jarrell-Ash Enviro II ICP. Calibration is achieved using a variety of international reference materials. Independent control standards are also analyzed.

2) Instrumental Neutron Activation Analysis (INAA) (Hoffman, 1992)

About 1 g powdered sample is weighed into small polyethylene vials specially fabricated for Actlabs for low background. Samples were irradiated with control international reference material CANMET WMS-1 and NiCr flux wires at a thermal neutron flux of 7×1012 n cm^{-2} s^{-1} in the McMaster Nuclear Reactor. Following a 7 day decay the samples are measured on Ortec high purity Ge detector with a resolution of 1.67 KeV for the 1332 KeV Co-60 photopeak. The detector is linked to Canberra Series 95 multichannel and is fully computer automated. Activities for each element are decay and weight corrected and compared to a detector calibration developed from multiple international certified reference materials. MRG-1 is used solely as a control to verify the system is operating properly. Selected samples are re-measured and compared to the original as part of the QA procedure.

3) X-ray Fluorescence (XRF)

The trace elements analyses are done on pressed powder pellets made from 6 g of sample. Spectral interferences are corrected from pre-calculated interfering factors. Because of the trace level (<1000 ppm) of the analyses, only the mass absorptions are corrected for matrix effects. The mass absorption coefficients are derived from measuring the Compton scatter of the Rh-tube. The background and mass absorption corrected intensities are then calculated against the calibrations constructed from 24 international geological reference materials. The limits of detection are between 1 and 5 ppm.

A.3. Laser Ablation ICP-MS was done by R.E. Hannigan

The LA-ICP-MS system used in this study (LITER-Old Dominion University) consists of a Nd:YAG (266-nm wavelength) laser connected to a double focusing sector field inductively coupled plasma mass spectrometer. Polished, uncovered thin sections were placed within the laser housing. The laser was pulsed at 10 Hz using 2 mJ energy. The material was ablated in an Argon atmosphere and entrained in Argon for analysis by ICP-MS. The isotopes ^{43}Ca, ^{51}V, ^{52}Cr, ^{63}Cu, ^{85}Rb, ^{88}Sr, ^{89}Y, ^{90}Zr, ^{137}Ba, ^{139}La, ^{140}Ce, ^{141}Pr, ^{146}Nd, ^{147}Sm, ^{151}Eu, ^{157}Gd, ^{159}Tb, ^{163}Dy, ^{165}Ho, ^{167}Er, ^{169}Tm, ^{173}Yb, ^{175}Lu, ^{208}Pb, ^{232}Th, and ^{238}U were measured with ^{43}Ca (0.135% Ca) used as an index isotope to compensate for variations in ablation yield due to porosity differences in the samples. Background and standard measurements were collected before and after the analysis of the samples to correct for instrument drift.

NIST glass standard SRM 612 was used to obtain concentration values for all elements. This standard has a nominal CaO concentration of 12% and measured concentrations between 30 and 40 ug/g for a suite of 61 elements (Pearce et al., 1997; Flem et al., 2002). The Oman samples are primarily chert and therefore the matrix of the samples is best matched by the NIST glass standard. Many laser ablation studies report accurate and precise results from different matrices using a suite of NIST standards, e.g. 612, 613, 614 and others (Horn et al., 1997; Flem et al., 2002). The technique used in this study provides reproducible quantitative concentrations (based on triplicate analyses of samples and standards) for V, Cr, Cu, Rb, Sr, Y, Zr, Ba, REE, Pb, Th, and U in the Oman sediments (Table 1). Based on multiple analyses of samples and NIST 612 the analytical error of the data is ~ 7%. Slightly higher errors (~ 10.2%) are associated with the REE due to the low concentration of these elements in chert. The detection limits of the LA-ICP-MS (Table 2), are defined as the concentration equivalent to three times the standard deviation of the background counts, as all of the analyses were accomplished in 1 day, between-day variation in detection limits is a non-issue.

A.4. Clay Mineral Analysis was done by G. Wilson

A Branson Model 450 sonifier was used to disaggregate the shale sample OMAN 5. About 10 g

of sample was placed in a 600 ml beaker and 300 ml of distilled water was added to the sample. The sample was sonified for 3 min and then allowed to settle for about 1 min before decanting the clay slurry through a 53 μm sieve into a glass settling jar. This step was repeated several times until the settling jar was filled. The jar was sufficiently deep to allow a settling depth of 15 cm and room below this depth for the silt fraction to collect. Using the principles of Stokes law a 12 h siphoning schedule was set up. The sample was shaken up and then allowed to settle. After 12 h the top 15 cm was siphoned off into a second settling jar. 10 ml of 0.5 M $MgCl_2$ was added to the second jar to flocculate the clay. The first settling jar was refilled with distilled water, shaken and again allowed to settle for 12 h. This siphoning procedure was repeated until sufficient clay had been separated to provide a representative clay sample for X-ray analysis. A 0.5 ml aliquot of the magnesium-saturated clay was washed once with approximately 5 ml of distilled water and centrifuged to settle the clay. The supernatant was discarded. The sample was then redispersed in 0.5 ml of distilled water and plated onto a glass X-ray disk. The disk was covered with a tray and allowed to dry overnight. A second 0.5 ml aliquot of magnesium saturated clay was treated 3 times with 5 ml of 1 M KCl to replace the magnesium with potassium, washed once with 5 ml of distilled water to remove excess potassium, as in the procedure for the magnesium-saturated sample. This sample was then dispersed in 0.5 ml of distilled water and plated onto a second glass slide and covered with a tray as in the procedure for the magnesium-saturated slide. The air-dried slides were X-rayed using a Rigaku Geigerflex DMAX II diffractometer. The samples were scanned from 3–35° two theta using a step width of 0.02° and a counting time of 4 s. The magnesium-saturated slide having been X-rayed was placed in a desiccator containing ethylene glycol, sealed and placed in an oven at 65 °C for 2 days before being scanned from 3–15° 2 theta. A sample of the shale was pulverized using a Retsch motorized mortar and pestle. The material was packed into an X-ray sample ring and scanned from 3–90° 2 theta using a step width of 0.02° and counting for 20 s. The diffractometer is equipped with a fine focus cobalt source which is operated at 1.0 kW powers (see Klute, 1986, pp. 392–396).

References

Allen, J.R.L., 1982. Sedimentary Structures: Their Character and Physical Basis, vol. 1. Elsevier, Amsterdam. 593 pp.

Béchennec, F., Le Metour, J., Rabu, D., Villey, M., Beurrier, M., 1988. The Hawasina Basin: a fragment of starved passive continental margin, thrust over the Arabian Platform during the obduction of the Semail Nappe. Tectonophysics 151, 323–343.

Ben-Menahem, A., Rosenman, M., 1972. Amplitude patterns of tsunami waves from submarine earthquakes. Journal of Geophysical Research 77, 3097–3128.

Blechschmidt, I. 2002. The Mesozoic Hamrat Duru Group (Oman Mountains)—Sedimentary and Structural Evolution of a Neo-Tethyan Passive Continental Margin. PhD thesis, Institut fur Geologie, Universitat Bern.

Blechschmidt, I., Dumitrica, P., Matter, A., Krystyn, L., Peters, Tj., 2004. Stratigraphic architecture of the northern Oman continental margin—Mesozoic Hamrat Dura Group, Hawasina complex, Oman. GeoArabia 9, 81–132.

Bondevik, S., Svendsen, J.I., Johnsen, G., Mangerud, J., Kaland, P.E., 1997. The Storegga tsunami along the Norwegian coast, its age and runup. Boreas 26, 29–54.

Bornhold, B.D., Fine, I.V., Rabinovich, A.B., Thomson, R.E., Kulikov, E.A., 2003. The Grand Banks landslide-generated tsunami of November 18, 1929: analysis and numerical modeling. Geophysical Research Abstracts 5, 1775.

Brookfield, M.E., 1977. The emplacement of giant ophiolite nappes 1, Mesozoic–Cenozoic examples. Tectonophysics 37, 247–303.

Bryant, E., 2001. Tsunami: The Underrated Hazard. Cambridge University Press, New York. 320 pp.

Carracedo, J.C., Day, S.J., Guillou, H., Torrado, F.J.P., 1999. Giant Quaternary landslides in the evolution of La Palma and El Hierro, Canary Islands. Journal of Volcanology and Geothermal Research 94, 169–190.

Coleman, P.J., 1968. Tsunamis as geological agents. Journal of the Geological Society of Australia 15, 267–273.

Condie, K., 1993. Chemical composition and evolution of the upper continental crust: Contrasting results from surface samples and shales. Chemical Geology 104, 1–37.

Cooper, D.J.W., 1988. Structure and sequence of thrusting in deep-water sediments during ophiolite emplacement in the south-central Oman Mountains. Journal of Structural Geology 10, 473–485.

Cooper, D.J.W., 1989. A longitudinal carbonate fan from the Jurassic of the Oman Mountains: the Guwayza Limestone Formation of the Hamrat ad Duru. Sedimentary Geology 61, 253–275.

Cooper, D.J.W., 1990. Sedimentary evolution and paleogeographical reconstruction of the Mesozoic continental rise in Oman: evidence from the Hamrat Duru Group. Geological Society Special Publication 49, 161–187.

Crevello, P.D., Schlager, W., 1980. Carbonate debris sheets and turbidites, Exuma Sound, Bahamas. Journal of Sedimentary Petrology 50, 1121–1148.

Dawson, A.G., 1999. Linking tsunami deposits, submarine slides and offshore earthquakes. Quaternary International 60, 119–126.

Duke, W.L., Arnott, R.W.C., Cheel, R.J., 1991. Shelf sandstones and hummocky cross-stratification: new insights on a stormy debate. Geology 6, 625–628.

Edwards, D.A., 1993. Turbidity Currents: Dynamics, Deposits and Reversals. Springer Verlag, Berlin. 173 pp.

Felletti, F., 2002. Complex bedding geometries and facies associations of the turbiditic fill of a confined basin in a transpressive setting (Castagnola Fm., Tertiary Piedmont Basin, NW Italy). Sedimentology 49, 645–667.

Felton, E.A., Crook, K.A.W., Keating, B.H., 2000. The Hulopoe Gravel, Lanai, Hawaii: new sedimentological data and their

bearing on the "giant wave" (mega-tsunami) emplacement hypothesis. Pure and Applied Geophysics 157, 1257–1284.

Flem, B., Larsen, R.B., Grimstvedt, A., Mansfeld, J., 2002. In situ analysis of trace elements in quartz by using laser ablation inductively coupled plasma mass spectrometry. Chemical Geology 182, 237–247.

Franceschelli, M., Puxeddu, M., Carcangui, G., Gattiglio, M., Pannuti, F., 1996. Breccia-hosted manganese-rich minerals of Alpi Apuane, Italy: a marine, redox-generated deposit. Lithos 37, 309–333.

Fritz, H.M., Hager, W.H., Minor, H.-E., 2001. Lituya Bay case: rockslide impact and wave run-up. Science of Tsunami Hazards 19, 3–22.

Gersonde, R., Kyte, F., Bleil, U., Diekmann, B., Flores, J.A., Gohl, K., Grahl, G., Hagen, R., Kuhn, G., Sierro, F.J., Volker, D., Abelmann, A., Bostwick, J.A., 1997. Geological record and reconstruction of the late Pliocene impact of the Eltanin asteroid in the Southern Ocean. Nature 390, 357–363.

Glennie, W.K., Boeuf, M.G.A., Hughes-Clarke, M.W., Moody-Stuart, M., Pilaar, W., Reinhardt, B.M., 1974. Geology of the Oman Mountains. Koninklijk Nederlands Geologisch Mijnbouwkundig Genootschap 50 (1), 1–423.

Haan, E., Corbin, S.G., Hughes Clarke, M.W., Mabillard, J.E., 1990. The Lower Kahmah Group of Oman: the carbonate fill of a marginal shelf basin. Geological Society Special Publication 49, 109–125.

Hallam, A., 2001. A review of the broad pattern of Jurassic sea-level changes and their possible causes in the light of current knowledge. Palaeogeography, Palaeoclimatology, Palaeoecology 167, 23–37.

Hannigan, R.E., Basu, A.R., 1998. Late Diagenetic Trace Element Remobilization in Organic-Rich Black Shales of the Taconic Foreland Basin of Québec, Ontario and New York. In: Schieber, J., Zimmerle, W., Sethi, P. (Eds.), Mudstones and Shales: Recent Progress in Shale Research. Schweizerbart'sche Verlagsbuchhandlung, Berlin, pp. 209–234.

Hartley, A., Howell, J., Mather, A.E., Chong, G., 2001. A possible Plio-Pleistocene tsunami deposit, Hornitos, northern Chile. Revista GeolwHgica de Chile 28, 1–18.

Haughton, P., 2001. Contained turbidites used to track sea bed deformation and basin migration, Sorbas Basin, southeast Spain. Basin Research 13, 117–139.

Hills, J.G., Mader, C.L., 1997. Tsunami produced by the impacts of small asteroids. Annals of the New York Academy of Sciences 822, 381–394.

Hoffman, E.L., 1992. Instrumental Neutron Activation in Geoanalysis. Journal of Geochemical Exploration 44, 297–319.

Horn, I., Hinton, R.W., Jackson, S.E., Longerich, S.A., 1997. Ultra-trace element analysis of NIST SRM 616 and 614 using laser ablation microprobe-inductively coupled plasma-mass spectrometry LAM-ICP-MS: a comparison with secondary ion mass spectrometry SIMS. Geostandards Newsletter 21, 191–203.

Keating, B.H., Helsey, C.E., 2002. The ancient shorelines of Lanai, Hawaii, revisited. Sedimentary Geology 150, 3–15.

Keating, B.H., McGuire, W.J., 2000. Island edifice failures and associated tsunami hazards. Pure and Applied Geophysics 157, 899–955.

Kennedy, J.F., 1969. The formation of sediment ripples, dunes, and antidunes. Annual Review of Fluid Mechanics 1, 147–168.

Klein, D. de V., Marsaglia, K.M., 1987. Discussion: hummocky cross-stratification, tropical hurricanes, and intense winter storms. Sedimentology 34, 333–359.

Klute, A. (Ed.), 1986. Methods of Soil Analysis. Part 1 Physical and Mineralogical Methods, 2nd edition. American Society of Agronomy, Madison, WI, pp. 383–411.

Kubo, Y., 2002. Laboratory experiments and numerical simulation of sediment wave formation by turbidity currents. Geological Society of America Annual Meeting, Denver Oct. 27–30, 2002. Paper no. 60-5.

Kuznetsov, V.G., 2003. Nekto-Planktonogenic Carbonate Formations and their evolution in the Earth's history. Lithology and Mineral Resources 37, 503–522.

Lee, H.J., Syvitski, J.P.M., Parker, G., Orange, D., Locat, J., Hutton, E. W.H., Imran, J., 2002. Distinguishing sediment waves from slope failure deposits: field examples, including the 'Humboldt slide' and modeling results. Marine Geology 192, 79–104.

Le Nindre, Y-M., Vaslet, D., Le Metour, J., Bertrand, J., Halawani, M., 2003. Subsidence modeling of the Arabian Platform from Permian to Paleogene outcrops. Sedimentary Geology 156, 263–285.

Mazumdar, A., Banerjee, D.N, Schidlowski, M., Balaram, V., 1999. Rare-earth elements and Stable Isotope Geochemistry of early Cambrian chert–phosphorite assemblages from the Lower Tal Formation of the Krol Belt (Lesser Himalaya, India). Chemical Geology 156, 275–297.

McMurtry, G.M., Watts, P., Fryer, G.J., Smith, J.R., Imamura, F., 2004. Giant landslides, mega-tsunamis, and paleo-sea level in the Hawaiian Islands. Marine Geology 203, 219–233.

Moore, J.G., Normark, W.R., Holcomb, R.T., 1994. Giant Hawaiian Landslides. Annual Review of Earth and Planetary Sciences 22, 119–144.

Mullins, H.T., Cook, H.E., 1986. Carbonate apron models: alternatives to the submarine fan model for paleoenvironmental analysis and hydrocarbon exploration. Sedimentary Geology 48, 37–79.

Mullins, H.T., Van Buren, H.M., 1979. Modern modified carbonate grain flow deposits. Journal of Sedimentary Petrology 48, 747–752.

Mullins, H.T., Gardulski, A.F., Hine, A.C., 1986. Catastrophic collapse of the west Florida carbonate platform margin. Geology 14, 167–170.

Murray, R.W., 1994. Chemical criteria to identify the depositional environment of chert: general principles and applications. Sedimentary Geology 90, 213–232.

Mutti, E., Ricci Luchi, F., Seguret, M., Zanzucchi, G., 1984. Seismoturbidites: a new group of resedimented deposits. Marine Geology 55, 103–116.

Myrow, P.M., Southard, J.B., 1996. Tempestite deposition. Journal of Sedimentary Research 66, 875–887.

Myrow, P.M., Fischer, W., Goodge, J.W., 2002. Wave-modified turbidites: combined-flow shoreline and shelf deposits, Cambrian, Antarctica. Journal of Sedimentary Research 72, 641–656.

Nemec, W., 1990. Aspects of sediment movement on steep delta slopes. Special Publication of the International Association of Sedimentologists 10, 29–74.

Pararas-Carayannis, G., 1999. Analysis of mechanisms of tsunami generation in Lituya Bay. Science of Tsunami Hazards 17, 193–206.

Pearce, N.J.G., Perkins, W.T., Westgate, J.W., Gorton, M.P., Jackson, S.E., Neal, C.R., Chenery, S.P., 1997. Compilation of new and published major and trace element data for NIST SRM 610 and NIST SRM 612 glass reference materials. Geostandards Newsletter 21, 115–144.

Pickering, K.T., Hiscott, R.N., 1985. Contained (reflected) turbidity currents from the Middle Ordovician Cloridorme Formation,

Quebec, Canada: an alternative to the antidune hypothesis. Sedimentology 32, 373–394.
Pillevuit, A., Marcoux, J., Stampfli, G., Baud, A., 1997. The Oman Exotics: a key to understanding of Neotethyan geodynamic evolution. Geodynamica Acta 10, 209–238.
Pinegina, T.K., Bourgeois, J., Bazanova, L.I., Melekestsev, I.V., Braitseva, O.A., 2003. A millenial-scale record of Holocene tsunamis on the Kronotskiy Bay coast, Kamchatka, Russia. Quaternary Research 59, 36–47.
Piper, D.J.W., Kontoupolis, N., 1994. Bedforms in submarine channels: comparison of ancient examples from Greece with studies of recent turbidite systems. Journal of Sedimentary Research 64, 247–252.
Pratt, B.R., 2002. Storms versus tsunamis: dynamic interplay of sedimentary, diagenetic, and tectonic processes in the Cambrian of Montana. Geology 30, 423–426.
Pratt, B.R., Smewing, J.D., 1990. Jurassic and Early Cretaceous platform margin configuration and evolution, central Oman Mountains. Geological Society Special Publication 49, 69–88.
Ricateau, R., Riche, P.H., 1980. Geology of the Musandam Peninsula (Sultanate of Oman) and its surroundings. Journal of Petroleum Geology 3, 139–152.
Robertson, A.H.F., 1987. The transition from a passive margin to an Upper Cretaceous foreland basin related to the ophiolite emplacement in the Oman Mountains. Geological Society of America Bulletin 99, 633–653.
Robertson, A.H.F., Searle, M.P., 1990. The northern Oman Tethyan continental margin: stratigraphy, structure, concepts and controversies. Geological Society Special Publication 49, 3–25.
Robertson, A.H.F., Blome, C.D., Cooper, D.J.W., Kemp, A.E.S., Searle, M.P., 1990a. Evolution of the Arabian continental margin in the Dibba Zone, Northern Oman Mountains. Geological Society Special Publication 49, 251–284.
Robertson, A.H.F., Kemp, A.E.S., Rex, D.C., Blome, C.D., 1990b. Sedimentary and structural evolution of a continental margin transform lineament: the Hatta Zone, Northern Oman Mountains. Geological Society Special Publication 49, 285–305.
Rubin, K.H., Fletcher III, C.H., Sherman, C., 2000. Fossiliferous Lana'i deposits formed by multiple events rather than a single giant tsunami. Nature 408, 675–681.
Searle, M.P., 1985. Sequence of thrusting and origin of culminations in the northern and central Oman Mountains. Journal of Structural Geology 7, 129–143.
Searle, M.P., Graham, G.M., 1982. "Oman exotics"—Oceanic carbonate build-ups associated with the early stages of continental rifting. Geology 10, 23–49.
Seilacher, A., Aigner, T., 1991. Storm deposition at the bed facies and basin scale: the geologic perspective. In: Einsele, G., Ricken, W., Seilacher, A. (Eds.), Cycles and Events in Stratigraphy. Springer Verlag, Berlin, pp. 249–267.
Shanmugam, G., Moiola, R., 1991. Types of submarine fan lobes: models and implications. American Association of Petroleum Geologists Bulletin 75, 156–179.
Shiki, T., Yamazaki, T., 1996. Tsunami-induced conglomerates in Miocene upper bathyal deposits, Chita Peninsula, central Japan. Sedimentary Geology 104, 175–188.
Silver, E., Day, S., Ward, S., Hoffmann, G., Llanes, P., Lyons, A., Driscoll, N., Perembo, R., John, S., Saunders, S., Tarani, F., Anton, L., Abiari, I., Applegate, B., Engels, J., Smith, J., Tagliodes, J., 2005. Island arc debris avalanches and tsunami generation. EOS. Transactions-American Geophysical Union 86 (47), 485–489.
Simonson, B.M., Glass, P., 2004. Spherule layers—records of ancient impacts. Annual Review of Earth and Planetary Sciences 32, 329–361.
Spence, G.H., Tucker, M.E., 1997. Genesis of limestone megabreccias and their significance in carbonate sequence stratigraphic models: a review. Sedimentary Geology 112, 163–193.
Tada, R., Nakano, Y., Iturralde-Vinent, M.A., Yamamoto, S., Kamata, T., Tajika, E., Toyoda, K., Kiyokawa, S., Garcia, D., Oji, T., Goto, K., Takayama, H., Rojas, R., Matsui, T., 2002. Complex tsunami waves suggested by the Cretaceous/Tertiary boundary deposits at Moncada section, western Cuba. Special Paper-Geological Society of America 356, 109–123.
Takashimizu, Y., Masuda, F., 2000. Depositional facies and sedimentary successions of earthquake-induced tsunami deposits in Upper Pleistocene incised valley fills, central Japan. Sedimentary Geology 135, 231–239.
Takayama, H., Tada, T., Matsui, T., Iturralde-Vinent, M.A., Oji, T., Tajika, E., Kiyokawa, S., Garcia, D., Okada, H., Hasegawa, T., Toyoda, K., 2000. Origin of the Penalver Formation in northwestern Cuba and its relation to K/T boundary impact events. Sedimentary Geology 135, 295–320.
Taylor, S.R., McLennan, S.M., 1985. The Continental Crust: Its Composition and Evolution. Blackwell Scientific Publications, Boston.
Tinti, S., Bortolucci, E., 2000. Analytical investigation on tsunamis generated by submarine slides. Annali di Geofisica 43, 519–536.
Todorovska, M.I., Hayir, A., Trifunac, M.D., 2002. A note on tsunami amplitudes above submarine slides and slumps. Soil Dynamics and Earthquake Engineering 22, 129–141.
Trifunac, M.D., Todorovska, M.I., 2002. A note on differences in tsunami source parameters for submarine slides and earthquakes. Soil Dynamics and Earthquake Engineering 22, 143–155.
Van den Berg, J.H., Van Gelder, A., Mastbergen, D.R., 2002. The importance of breaching as a mechanism of subaqueous slope failure in fine sand. Sedimentology 49, 81–95.
Walker, R.G., 1992. Turbidites and submarine fans. In: Walker, R.G., James, N.P. (Eds.), Facies Models: Response to Sea Level Change. Geological Association of Canada, St Johns, Newfoundland, pp. 239–263.
Ward, S.N., 2001. Landslide tsunami. Journal of Geophysical Research, [Solid Earth] 106, 11201–11215.
Watts, K.F., 1990. Mesozoic carbonate slope facies marking the Arabian platform margin in Oman: depositional history, morphology and palaeogeography. Geological Society Special Publication 49, 139–159.
Watts, K.F., 2003. Probabilistic analyses of landslide tsunami hazards. In: Locat, J., Meinert, J. (Eds.), Submarine Mass Movements and their Consequences. Kluwer Academic, Dordrecht, pp. 163–170.
Watts, K.F., Garrison, R.E., 1986. Sumeini Group, Oman—Evolution of a Mesozoic carbonate slope on a South Tethyan continental margin. Sedimentary Geology 48, 107–168.
Winchester, S., 2003. Krakatau: The Day the World Exploded August 27, 1883. Harper Collins, New York.
Wynn, R.B., Stow, D.A.V., 2002. Classification and characterization of deep-water sediment waves. Marine Geology 192, 7–22.
Wynn, R.B., Manson, D.G., Stow, D.A.V., Weaver, P.P.E., 2000. Turbidity current sediment waves on the submarine slopes of the western Canary Islands. Marine Geology 163, 185–198.
Yeats, R.S., Sieh, K., Clarence, R.A., 1997. The Geology of Earthquakes. Oxford University Press, New York.